solution, which contained 80 mM ATP, 800 μM 7-methylguanosine, and 0.1 unit/ml purine nucleoside phosphorylase. The latter two components were used to eliminate contaminating Pi. Changes in the fluorescence at 466 nm were monitored continuously with a fluorometer (F-4500, Hitachi).

ADP Release

Release of ADP from GroEL was measured spectrophotometrically with an ATP-regenerating system (Pullman et al., 1960; Kato et al., 1995). The assay mixture consisted of buffer A containing 0.2 mM NADH, 5 mM phosphoenolpyruvate, 100 μg/ml pyruvate kinase, 100 μg/ml lactate dehydrogenase, 2.5 mM DTT, and 1 mM ATP in the presence or absence of 1.4 μM GroES. MDH (47 μM) denatured in 6 M urea was diluted into the assay mixture to a final concentration of 1.0 μM. After 1 min, the reaction was initiated by injection of GroEL into the vigorously stirred solution. The decreases in the absorbance at 340 nm, due to oxidation of NADH, were monitored continuously with a spectrophotometer (V-550, Jasco, Japan).

Acknowledgments

We thank A. Horwich for critical discussion; M. Webb and T. Masaike for the use of the Pi binding protein assay; J. Suzuki and A. Koike for technical assistance; and R. Shiurba for comments on the manuscripts. This work was supported in part by Grants-in-Aid for Scientific Research on Priority Areas (to H.T. and M.Y.), Specially Promoted Research, COE research, the 21th Century COE program (to T.F.), and Scientific Research B (to H.T. and T.F.), from the Ministry of Education, Culture, Sports, Science, and Technology of Japan.

Received: October 2, 2003
Revised: March 29, 2004
Accepted: March 30, 2004
Published: May 20, 2004

References

Aoki, K., Taguchi, H., Shindo, Y., Yoshida, M., Ogasahara, K., Yutani, K., and Tanaka, N. (1997). Calorimetric observation of a GroEL-protein binding reaction with little contribution of hydrophobic interaction. J. Biol. Chem. *272*, 32158–32162.

Boisvert, D.C., Wang, J., Otwinowski, Z., Horwich, A.L., and Sigler, P.B. (1996). The 2.4 Å crystal structure of the bacterial chaperonin GroEL complexed with ATPgS. Nat. Struct. Biol. *3*, 170–177.

Braig, K., Otwinowski, Z., Hegde, R., Boisvert, D.C., Joachimiak, A., Horwich, A.L., and Sigler, P.B. (1994). The crystal structure of the bacterial chaperonin GroEL at 2.8 Å. Nature *371*, 578–586.

Brune, M., Hunter, J.L., Corrie, J.E., and Webb, M.R. (1994). Direct, real-time measurement of rapid inorganic phosphate release using a novel fluorescent probe and its application to actomyosin subfragment 1 ATPase. Biochemistry *33*, 8262–8271.

Brune, M., Hunter, J.L., Howell, S.A., Martin, S.R., Hazlett, T.L., Corrie, J.E., and Webb, M.R. (1998). Mechanism of inorganic phosphate interaction with phosphate binding protein from Escherichia coli. Biochemistry *37*, 10370–10380.

Bukau, B., and Horwich, A.L. (1998). The Hsp70 and Hsp60 chaperone machines. Cell *92*, 351–366.

Burston, S.G., Ranson, N.A., and Clarke, A.R. (1995). The origins and consequences of asymmetry in the chaperonin reaction cycle. J. Mol. Biol. *249*, 138–152.

Chaudhry, C., Farr, G.W., Todd, M.J., Rye, H.S., Brunger, A.T., Adams, P.D., Horwich, A.L., and Sigler, P.B. (2003). Role of the gamma-phosphate of ATP in triggering protein folding by GroEL-GroES: function, structure and energetics. EMBO J. *22*, 4877–4887.

Chen, L., and Sigler, P.B. (1999). The crystal structure of a GroEL/peptide complex: plasticity as a basis for substrate diversity. Cell *99*, 757–768.

Chen, J., Walter, S., Horwich, A.L., and Smith, D.L. (2001). Folding of malate dehydrogenase inside the GroEL-GroES cavity. Nat. Struct. Biol. *8*, 721–728.

Cliff, M.J., Kad, N.M., Hay, N., Lund, P.A., Webb, M.R., Burston, S.G., and Clarke, A.R. (1999). A kinetic analysis of the nucleotide-induced allosteric transitions of GroEL. J. Mol. Biol. *293*, 667–684.

Ewalt, K.L., Hendrick, J.P., Houry, W.A., and Hartl, F.U. (1997). In vivo observation of polypeptide flux through the bacterial chaperonin system. Cell *90*, 491–500.

Fenton, W.A., Kashi, Y., Furtak, K., and Horwich, A.L. (1994). Residues in chaperonin GroEL required for polypeptide binding and release. Nature *371*, 614–619.

Geladopoulos, T.P., Sotiroudis, T.G., and Evangelopoulos, A.E. (1991). A malachite green colorimetric assay for protein phosphatase activity. Anal. Biochem. *192*, 112–116.

Hartl, F.U., and Hayer-Hartl, M. (2002). Molecular chaperones in the cytosol: from nascent chain to folded protein. Science *295*, 1852–1858.

Horwich, A.L., Low, K.B., Fenton, W.A., Hirshfield, I.N., and Furtak, K. (1993). Folding in vivo of bacterial cytoplasmic proteins: role of GroEL. Cell *74*, 909–917.

Houry, W.A., Frishman, D., Eckerskorn, C., Lottspeich, F., and Hartl, F.U. (1999). Identification of in vivo substrates of the chaperonin GroEL. Nature *402*, 147–154.

Hunt, J.F., Weaver, A.J., Landry, S.J., Gierasch, L., and Deisenhofer, J. (1996). The crystal structure of the GroES co-chaperonin at 2.8 Å resolution. Nature *379*, 37–45.

Kato, Y., Sasayama, T., Muneyuki, E., and Yoshida, M. (1995). Analysis of time-dependent change of Escherichia coli F1-ATPase activity and its relationship with apparent negative cooperativity. Biochim. Biophys. Acta *1231*, 275–281.

Kawata, Y., Kawagoe, M., Hongo, K., Miyazaki, T., Higurashi, T., Mizobata, T., and Nagai, J. (1999). Functional communications between the apical and equatorial domains of GroEL through the intermediate domain. Biochemistry *38*, 15731–15740.

Makino, Y., Amada, K., Taguchi, H., and Yoshida, M. (1997). Chaperonin-mediated folding of green fluorescent protein. J. Biol. Chem. *272*, 12468–12474.

Mayhew, M., da Silva, A.C.R., Martin, J., Erdjument-Bromage, H., Tempst, P., and Hartl, F.U. (1996). Protein folding in the central cavity of the GroEL-GroES chaperonin complex. Nature *379*, 420–426.

Miyazaki, T., Yoshimi, T., Furutsu, Y., Hongo, K., Mizobata, T., Kanemori, M., and Kawata, Y. (2002). GroEL-substrate-GroES ternary complexes are an important transient intermediate of the chaperonin cycle. J. Biol. Chem. *277*, 50621–50628.

Motojima, F., Makio, T., Aoki, K., Makino, Y., Kuwajima, K., and Yoshida, M. (2000). Hydrophilic residues at the apical domain of GroEL contribute to GroES binding but attenuate polypeptide binding. Biochem. Biophys. Res. Commun. *267*, 842–849.

Peralta, D., Hartman, D.J., Hoogenraad, N.J., and Hoj, P.B. (1994). Generation of a stable folding intermediate which can be rescued by the chaperonins GroEL and GroES. FEBS Lett. *339*, 45–49.

Pullman, M.E., Penefsky, H.S., Datta, A., and Racker, E. (1960). Partial resolution of the enzymes catalyzing oxidative phosphorylation. J. Biol. Chem. *235*, 3322–3329.

Rye, H.S., Burston, S.G., Fenton, W.A., Beechem, J.M., Xu, Z., Sigler, P.B., and Horwich, A.L. (1997). Distinct actions of *cis* and *trans* ATP within the double ring of the chaperonin GroEL. Nature *388*, 792–798.

Rye, H.S., Roseman, A.M., Chen, S., Furtak, K., Fenton, W.A., Saibil, H.R., and Horwich, A.L. (1999). GroEL-GroES cycling: ATP and nonnative polypeptide direct alternation of folding-active rings. Cell *97*, 325–338.

Saibil, H.R., and Ranson, N.A. (2002). The chaperonin folding machine. Trends Biochem. Sci. *27*, 627–632.

Sakikawa, C., Taguchi, H., Makino, Y., and Yoshida, M. (1999). On the maximum size of proteins to stay and fold in the cavity of GroEL underneath GroES. J. Biol. Chem. *274*, 21251–21256.

Shtilerman, M., Lorimer, G.H., and Englander, S.W. (1999). Chaperonin function: folding by forced unfolding. Science *284*, 822–825.

Sigler, P.B., Xu, Z., Rye, H.S., Burston, S.G., Fenton, W.A., and Horwich, A.L. (1998). Structure and function in GroEL-mediated protein folding. Annu. Rev. Biochem. *67*, 581–608.

Taguchi, H., Ueno, T., Tadakuma, H., Yoshida, M., and Funatsu, T. (2001). Single-molecule observation of protein-protein interactions in the chaperonin system. Nat. Biotechnol. *19*, 861–865.

Thirumalai, D., and Lorimer, G.H. (2001). Chaperonin-mediated protein folding. Annu. Rev. Biophys. Biomol. Struct. *30*, 245–269.

Todd, M.J., Viitanen, P.V., and Lorimer, G.H. (1994). Dynamics of the chaperonin ATPase cycle: implications for facilitated protein folding. Science *265*, 659–666.

Viani, M.B., Pietrasanta, L.I., Thompson, J.B., Chand, A., Gebeshuber, I.C., Kindt, J.H., Richter, M., Hansma, H.G., and Hansma, P.K. (2000). Probing protein-protein interactions in real time. Nat. Struct. Biol. *7*, 644–647.

Viitanen, P.V., Gatenby, A.A., and Lorimer, G.H. (1992). Purified GroEL interacts with the non-native states of a multitude of E. coli proteins. Protein Sci. *1*, 361–369.

Weissman, J.S., Hohl, C.M., Kovalenko, O., Kashi, Y., Chen, S., Braig, K., Saibil, H.R., Fenton, W.A., and Horwich, A.L. (1995). Mechanism of GroEL action: productive release of polypeptide from a sequestered position under GroES. Cell *83*, 577–587.

Weissman, J.S., Rye, H.S., Fenton, W.A., Beechem, J.M., and Horwich, A.L. (1996). Characterization of the active intermediate of a GroEL-GroES-mediated protein folding reaction. Cell *84*, 481–490.

Wu, P.G., and Brand, L. (1994). Resonance energy transfer: methods and applications. Anal. Biochem. *218*, 1–13.

Xu, Z., Horwich, A.L., and Sigler, P.B. (1997). The crystal structure of the asymmetric GroEL-GroES-(ADP)7 chaperonin complex. Nature *388*, 741–750.

distal regions of the coiled-coils partially expose hydrophobic patches, and there is evidence that coiled-coils are required for the multivalent binding of non-native proteins (23). Eukaryotic prefoldin possesses a structure similar to that of archaeal prefoldin and has been observed to capture a substrate protein (actin) in the cavity formed by its six "tentacles" (24). In the three-dimensional reconstitution of the prefoldin-actin complex, actin appears to interact with prefoldin in a region that is not well defined but is also consistent with the distal regions of the coiled-coils (24). Additional evidence for actin and tubulin substrate interaction with the distal ends of different but overlapping sets of eukaryotic prefoldin subunits has been obtained recently (25).

In contrast, the interaction and functional cooperation between the archaeal chaperonin and prefoldin is comparably less understood. The archaeal chaperones represent a powerful model system for examining their functional cooperation because of their simple subunit composition and structural stability.

We have already reported that the prefoldin from *Pyrococcus horikoshii* OT3 (PhPFD) functionally cooperates with chaperonins in the refolding of the green fluorescent protein (GFP) *in vitro* (26). In the present study, we have examined the interaction between a prefoldin and a chaperonin from hyperthermophilic archaea by immunoprecipitation, single molecule observation, and surface plasmon resonance, and characterized the substrate and chaperonin binding site of prefoldin. Our results reveal that both the distal N- and C-terminal regions of the β subunit are important for substrate binding and also for interaction with a chaperonin. Importantly, the dual function of the prefoldin tips (substrate and chaperonin binding) may represent an important property that facilitates the functional cooperation with a chaperonin.

EXPERIMENTAL PROCEDURES

Plasmids, Bacterial Strains, and Reagents—The plasmid pT7Blue T (Novagen) was used for cloning and DNA sequencing of the gene. The plasmid pET23b (Novagen) was used for construction of the expression system. *Escherichia coli* strains used in this study were DH5α for the preparation of plasmids and BL21(DE3) for expression. Site-directed mutagenesis was performed using a QuikChange site-directed mutagenesis kit (Stratagene). Restriction enzymes, Ex *Taq*DNA polymerase and other reagents for gene manipulation were purchased from Takara Bio Inc. (Shiga, Japan). Citrate synthase (CS) from porcine heart, bovine serum albumin, glucose oxidase, and catalase were purchased from Sigma. All other chemicals were of analytical grade, and solutions were made up in ultrapure water.

Proteins—Both wild-type and mutated PhPFDs were prepared by reconstitution from purified subunits. Truncation mutant genes were prepared by PCR amplification from the wild-type gene using the primers (wtα, PH0527Fw 5′-CAT-ATG-ATA-AGG-ATG-GCT-CAG-AA-3′, PH0527Rv 5′-GGA-TCC-CTAC-TTC-TTA-ACC-TTA-AAG-C-3′; tc8α, PH0527Fw, PH0527tc8Rv 5′-TTG-GAT-CCC-TAA-CTT-TGC-TTT-TGC-TGT-A-3′; tn17α, PH0527tn17Fw 5′CAT-ATG-TAC-CAG-GTT-TTA-CAA-GCT-CAA-G-3′, PH0527Rv; wtβ, PH0532Fw 5′-CAT-ATG-CAG-AAC-ATT-CCT-CCC-CA-3′, PH0532Rv 5′-GTC-GAC-TCA-GCC-AGC-GGT-AGG-CGG-CC-3′; tc5β, PH0532Fw, PH0532tc5Rv 5′-GTC-GAC-TCA-CCT-CAG-AGC-GGC-TTG-AAT-CTT-3′; tc6β, PH0532Fw, PH0532tc6Rv 5′-GTC-GAC-TCA-CAG-AGC-GGC-TTG-AAT-CTT-CTG-3′; tc7β, PH0532Fw, PH0532tc7Rv 5′-GTC-GAC-TCA-AGC-GGC-TTG-AAT-CTT-CTG-AG-3′; tc8β, PH0532Fw, PH0532tc8Rv 5′-TTG-TCG-ACT-CAG-GCT-TGA-ATC-TTC-TGA-G-3′; tn10β, PH0532tn10Fw 5′-CAT-ATG-CTT-GGC-CAA-CTC-GAT-ACG-TAT-C-3′, PH0532Rv). The constructs were designated according to the terminus, number of residues, and subunit type that was mutagenized, as exemplified by tc8α, a mutant α subunit with an 8-amino acid truncation from the C terminus, and tn17α, a mutant α subunit of with a 17-amino acid truncation from the N terminus. The amplified DNA for the truncation mutant was cloned into pT7Blue T. After sequence confirmation, the gene was excised with NdeI and BamHI (α subunit) or NdeI and SalI (β subunit), and inserted into pET23b. A mutant β subunit, L111A, denoting an amino acid substitution of Leu^{111} by Ala, was prepared by a QuikChange site-directed mutagenesis kit using the primers (PH0532L111AFw 5′-GAT-TCA-AGC-CGC-TGC-GAG-GCC-GCC-TAC-CGC-3′, PH0532L111ARv 5′-GCG-GTA-GGC-GGC-CTC-GCA-GCG-GCT-TGA-ATC-3′). The construct was also verified by DNA sequencing.

Each subunit was expressed in *E. coli* BL21(DE3). After removal of most *E. coli* proteins by heat treatment at 80 °C for 30 min, it was purified by anion exchange chromatography on a DEAE-Toyopearl column (Tosoh, Tokyo, Japan) using buffer A (50 mM Tris-HCl, pH 8.0, 0.1 mM EDTA) with a gradient of NaCl, and subsequent gel filtration on a HiLoad 26/60 Superdex 200 prep grade column (Amersham Biosciences) equilibrated with buffer A containing 150 mM NaCl. PhPFD complexes were reconstituted by incubating the mixture of the purified α and β subunits at the molar ratio of 1:2 at 80 °C for 30 min. The reconstituted complex was purified by gel filtration on a Bio-Prep column (Bio-Rad). The purified complex contained α and β subunits at the molar ratio of 1:2 as judged by SDS-PAGE analysis.

Chaperonins from *Pyrococcus horikoshii* OT3 (PhCPN), *Thermococcus* sp strain KS-1 (TkCPN), and *Thermus thermophilus* HB8 (TthCPN) were expressed and purified as described previously (17, 26).[2] Wild-type prefoldin from *M. thermoautotrophicum*, MtPFD, was prepared as described previously (22).

The GFP used in this report is a heat-stable mutant, with alanine inserted in the N-terminal region, a His tag in the C-terminal region, and amino acid substitution of F99S, M153T, V163A, and L165F (5, 27). It was purified as described previously (28).

Immunoprecipitation of Prefoldin with Anti-chaperonin Antibody—The immunoprecipitation experiments were performed using IMMUNOcatcher (CytoSignal) to examine the interactions between the prefoldin and the chaperonin in the presence or absence of denatured GFP. The anti-TkCPN antibody was used for the immunoprecipitation. Because of the high sequence homology between TkCPN and PhCPN, the anti-TkCPN antibody can specifically immunoprecipitate PhCPN. The preparation and purification of the antibody were described previously (29). The sample solutions for the immunoprecipitation containing 7.0 μM PhPFD and 10 mM HCl-unfolded GFP (at the specified concentration) were mixed and incubated at 65 °C for 10 min prior to the addition of 1.4 μM PhCPN. The samples were incubated at 65 °C for an additional 10 min. Then, 10 μl of anti-TkCPN antibody was added to 210 μl of the sample solution and incubated for 1 h at room temperature. Protein A/G resin (10 μl) was then applied to the mixture and incubated for 45 min. Proteins bound to the resin were collected by centrifugation, washed, and resuspended in SDS-PAGE sample solution. After incubation for 15 min, the bound proteins were collected by centrifugation and then analyzed by SDS-PAGE.

Preparation of Fluorescent-labeled Proteins—We prepared a mutant TkCPN with amino acid replacement of Asn^{472} by cysteine (TkCPN472C). This mutation site was selected on the basis of the criterion that the residue is fully exposed to solvent, minimizing the effect on the function of the chaperonin. TkCPN472C was treated with 5 mM dithiothreitol to reduce the cysteine residue. Dithiothreitol was removed by gel filtration on a Sephadex G-25 column (Amersham Biosciences) equilibrated with buffer B (25 mM HEPES-KOH, pH 7.4, 100 mM KCl, 5 mM $MgCl_2$). TkCPN472C was labeled with Alexa Fluor 488 C_5 maleimide (Alexa488, Molecular Probes) for 30 min at room temperature. PhPFD was labeled with Cy5 Mono-reactive Dye (Amersham Biosciences) by incubation for 1 h at room temperature. Amino groups of PhPFD were modified with Cy5. The labeled TkCPN472C (488-TkCPN) and PhPFD (Cy5-PhPFD) were separated from the unreacted reagents by gel filtration. The extent of labeling was determined by adsorption spectroscopy. The molar ratios of Alexa488 to TkCPN (16-mer) and that of Cy5 to PhPFD (6-mer) were 2.6 and 0.9, respectively. The 488 labeled TkCPN showed the same ATPase activity as that of the non-labeled TkCPN472C (data not shown). Cy5-PhPFD exhibited nearly the same activity in protecting CS from thermally induced aggregation compared with non-labeled PFD (data not shown).

Single-molecule Imaging of CPN·PFD Complex—100 nM 488-TkCPN was incubated with 100 nM Cy5-PhPFD at 60 °C for 10 min in buffer A. The resulting solution was diluted by 100-fold (*i.e.* 1 nM complex) with buffer A containing the oxygen scavenger system (25 mM glucose, 2.5 μM glucose oxidase, 10 nM catalase, and 10 mM dithiothreitol) and flowed into a flow cell made from a glass slide and coverslip for the successive fluorescent observation at room temperature.

The positions of individual 488-TkCPN and Cy5-PhPFD molecules adsorbed on the glass slide were visualized by total internal reflection fluorescence microscopy (TIRFM) (30). 488-TkCPN molecules were il-

[2] M. Okochi, H. Matsuzaki, T. Nomura, N. Ishii, and M. Yohda, manuscript in preparation.

THE JOURNAL OF BIOLOGICAL CHEMISTRY
Vol. 279, No. 30, Issue of July 23, pp. 31788–31795, 2004
Printed in U.S.A.

Kinetics and Binding Sites for Interaction of the Prefoldin with a Group II Chaperonin

CONTIGUOUS NON-NATIVE SUBSTRATE AND CHAPERONIN BINDING SITES IN THE ARCHAEAL PREFOLDIN*

Received for publication, March 15, 2004, and in revised form, May 6, 2004
Published, JBC Papers in Press, May 15, 2004, DOI 10.1074/jbc.M402889200

Mina Okochi‡§, Tomoko Nomura‡§, Tamotsu Zako‡, Takatoshi Arakawa‡, Ryo Iizuka‡, Hiroshi Ueda¶, Takashi Funatsu‖, Michel Leroux‡‡, and Masafumi Yohda‡§§**

*From the ‡Department of Biotechnology and Life Science, Tokyo University of Agriculture and Technology, 2-24-16, Naka-cho, Koganei, Tokyo 184-8588, Japan, the ¶Department of Chemistry and Biotechnology, School of Engineering, The University of Tokyo, 7-3-1 Hongo Bunkyo-ku, Tokyo 113-8656, Japan, the ‖Department of Physics, School of Science and Engineering, Waseda University, 3-4-1 Okubo, Tokyo 169-8555, Japan, and the **Department of Molecular Biology and Biochemistry, Simon Fraser University, Burnaby, British Columbia V5A 1S6, Canada*

Prefoldin is a jellyfish-shaped hexameric co-chaperone of the group II chaperonins. It captures a protein folding intermediate and transfers it to a group II chaperonin for completion of folding. The manner in which prefoldin interacts with its substrates and cooperates with the chaperonin is poorly understood. In this study, we have examined the interaction between a prefoldin and a chaperonin from hyperthermophilic archaea by immunoprecipitation, single molecule observation, and surface plasmon resonance. We demonstrate that *Pyrococcus* prefoldin interacts most tightly with its cognate chaperonin, and vice versa, suggesting species specificity in the interaction. Using truncation mutants, we uncovered by kinetic analyses that this interaction is multivalent in nature, consistent with multiple binding sites between the two chaperones. We present evidence that both N- and C-terminal regions of the prefoldin β subunit are important for molecular chaperone activity and for the interaction with a chaperonin. Our data are consistent with substrate and chaperonin binding sites on prefoldin that are different but in close proximity, which suggests a possible handover mechanism of prefoldin substrates to the chaperonin.

Molecular chaperones are ubiquitous proteins that are required for the correct folding, assembly, transport, and degradation of proteins within the cell (1). One class of chaperones, termed chaperonins, are seven- to nine-membered double ring complexes of 800–1000 kDa that capture non-native proteins in their central cavity to promote correct folding in an ATP-dependent manner (2–5). They are classified into two groups, group I found in bacteria and organelles of eukaryotes, and group II in archaea and in the cytoplasm of eukaryotes (6, 7). The bacterial group I chaperonin, GroEL, is a cylinder-shaped tetradecamer that is capped by the heptameric co-chaperone, GroES (8–10). In contrast, the group II chaperonin exists as an eight- or nine-rotationally symmetric double ring in a toroidal structure composed of homologous subunits of about 60 kDa and functions independently of a co-chaperone corresponding to GroES (11, 12). The crystal structures of the group II chaperonins from the acidothermophilic archaeum *Thermoplasma acidophilum* and the hyperthermophilic archaeum *Thermococcus* sp. strain KS-1 suggest that the long helical protrusions located at the opening of their cavities, in their apical domains, play the equivalent role of GroES as a built-in lid of the cavity (13–15). The archaeal chaperonin takes an open conformation in the nucleotide-free or ADP-bound states and changes to a closed conformation upon binding ATP (16, 17). Interestingly, closure of the built-in lid of CCT,[1] the eukaryotic cytosol group II chaperonin, is induced not by the binding but by the hydrolysis of ATP (18).

The group II chaperonins cooperate with a co-chaperone, prefoldin/GimC (19–21). Prefoldin (PFD) has been shown to participate in the maturation of actin and members of the tubulin family by transferring them in the incompletely folded states to CCT. Although there is neither actin nor tubulin in archaea, both prefoldin homologues and group II chaperonins have invariably been identified in all archaeal species (21, 22). Archaeal prefoldin consists of only two species of subunits, namely α and β, whereas eukaryotic prefoldins are composed of two different but related α class subunits and four related β class subunits. The crystal structure of the archaeal prefoldin from *Methanobacterium thermoautotrophicum* (MtPFD) has been determined at a resolution of 2.3 Å (23). It resembles a jellyfish in that its body consists of a double β-barrel assembly with six long tentacle-like coiled-coils protruding from it. The

* This work was supported in part by grants-in-aid for scientific research on priority areas (13033008, 14037216, and 15032212) and a grant of the National Project on Protein Structural and Functional Analyses from the Ministry of Education, Science, Sports and Culture of Japan (to M. Y.). The work reported here is a part of the 21st Century COE (Center of Excellence) program of "Future Nano-Materials" research and education project, which is financially supported by the Ministry of Education, Science, Sports, Culture, and Technology through Tokyo University of Agriculture & Technology. The costs of publication of this article were defrayed in part by the payment of page charges. This article must therefore be hereby marked "*advertisement*" in accordance with 18 U.S.C. Section 1734 solely to indicate this fact.

§ Both authors contributed equally to this work.

‡‡ Supported by the Canadian Institutes of Health Research (CIHR) and the Michael Smith Foundation for Health Research scholarship awards.

§§ To whom correspondence should be addressed. Tel./Fax: 81-42-388-7479; E-mail: yohda@cc.tuat.ac.jp.

[1] The abbreviations used are: CCT, cytosolic chaperonin containing TCP-1; PFD, prefoldin; PhCPN, chaperonin from *P. horikoshii* OT3; PhPFD, prefoldin from *P. horikoshii* OT3; MtPFD, prefoldin from *M. thermoautotrophicum*; GFP, green fluorescent protein; CS, citrate synthase from porcine heart; SPR, surface plasmon resonance; TkCPN, α chaperonin from *Thermococcus* sp. strain KS-1; TthCPN, chaperonin from *T. thermophilus* HB8; wtα, wild-type PhPFD α subunit; wtβ, wild-type PhPFD β subunit; TIRFM, total internal reflection fluorescence microscopy; RU, resonance unit(s).

luminated with a semiconductor laser (6.0 milliwatts, 473 nm, model ML0250A; Nippon Avionic Co. Inc., Tokyo, Japan). Cy5-PhPFD molecules were illuminated with a He-Ne laser (2.8 milliwatts, 632.8 nm, model GLG5350; NEC Co., Tokyo, Japan). The fluorescence emission from the specimen was collected with an oil-immersion microscope objective (1.40 numerical objective, ×100, PlanApo; Olympus, Tokyo, Japan). Images were taken by a silicon-intensified tube camera (C2400–08, Hamamatsu Photonics, Shizuoka, Japan) coupled to an image intensifier (VS4-1845, Video Scope International) and recorded on videotapes for subsequent analysis. At least two fields of images were recorded for each assay, and statistical analysis was made from five independent assays. The positions of 488-TkCPN and Cy5-PhPFD at the same fields were marked individually using Scion Image software (Scion Corp.).

Surface Plasmon Resonance Detection of Prefoldin-Chaperonin Interaction—The surface plasmon resonance experiments were performed with a Biacore J biosensor system (Biacore AB, Uppsala, Sweden) at the sensor temperature of 25 °C. PhPFD or PhCPN was coupled to the sensor chip (CM5 research grade) via standard *N*-hydroxysuccinimide and *N*-ethyl-*N*-(dimethylaminopropyl)carbodiimide activation. For immobilizing chaperonins, 190 μl of 50 μg/ml protein in 10 mM sodium acetate (pH 5.0) was injected on the sensor surface. 190 μl of 6 μg/ml prefoldin in 10 mM potassium phosphate buffer (pH 7.5) was injected on the sensor surface to immobilize prefoldin. Ethanolamine was then injected to quench the unreacted *N*-hydroxysuccinimide groups. The mobile phase buffer used was HBS-EP buffer (10 mM HEPES, pH 7.4, 150 mM NaCl, 3 mM EDTA, and 0.005% surfactant P-20). Analytes were injected at various concentrations, and the bound analytes were removed by washing with buffer 180 s after the injection.

Kinetic Analysis of Sensorgram Data—Kinetic constants were calculated from the sensorgram with BIAevaluation software, version 3.1 (Biacore), according to the global fitting model. The response curves for various analyte concentrations were globally fitted to several binding models provided with the above software. Apparent rate constants (k_{on1} and k_{off1} for the first step; k_{on2} and k_{off2} for the second step) were calculated based on the best fitted model, the bivalent model (first step: $L + A \leftrightarrow L \cdot A$; second step: $L \cdot A + L \leftrightarrow L_2 \cdot A$ (L: ligand, A: analyte)). Dissociation constants (K_D) were calculated by the resonance unit at equilibrium using the equation, $R_{eq} = R_{max} \cdot C/(C + K_D)$, where R_{eq} is equilibrium resonance units, R_{max} is the resonance signal at saturation, and C is the concentration of free analyte. By dividing the K_D values by that for the wild-type PhPFD, relative K_D values were calculated.

Thermal Aggregation Measurements of CS—Thermal aggregation of CS from porcine heart was monitored by measuring the light scattering at 500 nm with a spectrofluorophotometer (RF-5300PC, Shimadzu, Kyoto, Japan) at 50 °C with continuous stirring. Monitoring started after addition of CS (80 nM as a monomer) to 50 mM Tris-HCl buffer, pH 8.0, with or without 240 nM of wild-type or mutant PhPFD complexes preincubated at 50 °C. Activity for protecting CS from thermal aggregation was defined as the relative reduction of light scattering by the presence of PhPFD complexes after 200 s.

Fluorometric Monitoring of GFP Refolding—The refolding of GFP denatured in 12.5 mM HCl was monitored by the fluorescence at 510 nm with excitation at 396 nm using a spectrofluorophotometer (RF-5300PC). Fluorescent measurements were initiated with the addition of 15 μM native or acid-denatured GFP (10 μl) into 1.5 ml of dilution buffer (50 mM Tris-HCl, pH 8.0, 100 mM KCl, 5 mM dithiothreitol, and 25 mM $MgCl_2$) at 60 °C and under continuous stirring. To observe the chaperone activities, PhPFD complexes were added in the dilution buffer at a molar ratio of 1:5 (denatured GFP:prefoldin). Activity for arresting GFP refolding was defined as the relative reduction of fluorescence by the presence of PhPFD complexes after 600 s.

Other Methods—Proteins were analyzed by polyacrylamide gel electrophoresis on polyacrylamide gels containing SDS (SDS-PAGE) or polyacrylamide gels without SDS (Native-PAGE). Gels were stained with Coomassie Brilliant Blue R-250. Protein concentrations were measured by the method of Bradford with bovine serum albumin as the standard (31).

RESULTS

Substrate-independent Interaction of Archaeal Prefoldin with Its Chaperonin—A major question regarding the functional nature of the interaction between prefoldin and its cognate chaperonin is whether ternary complexes involving a substrate protein are required for efficient prefoldin-chaperonin interactions to take place. A potential affinity between the chaperonin and prefoldin from *P. horikoshii* (PhCPN and PhPFD, respectively), in the presence or absence of a denatured substrate protein, was investigated using immunoprecipitation experiments. Using purified chaperone components, immunoprecipitations were carried out with an antibody (anti-TkCPN), which specifically recognizes PhCPN, and analyzed by SDS-PAGE (Fig. 1). In the absence of the denatured protein substrate, an interaction between PhPFD and PhCPN was observed (Fig. 1, *lane 5*). In contrast, a control experiment showed that only a trace amount of PhPFD was immunoprecipitated by anti-chaperonin antibody in the absence of PhCPN (*lane 6*). When PhCPN was mixed with PhPFD preincubated with acid-denatured GFP (a known substrate for PhPFD; see Ref. 26), both PhPFD and the denatured GFP were co-precipitated with PhCPN (*lane 3*). Even in the presence of excess denatured GFP (final concentration; 21 μM), the amount of co-precipitated PhPFD was not altered (*lane 4*). Together, these results suggest that the archaeal prefoldin directly interacts with the chaperonin and that the interaction is not substantially affected by the presence of denatured proteins.

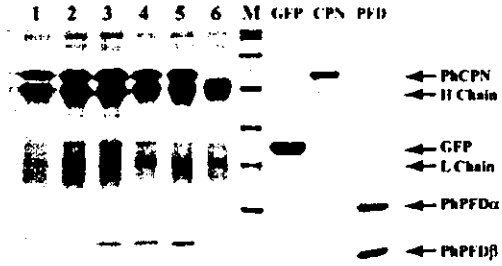

FIG. 1. ***In vitro* immunoprecipitation of prefoldin with anti-chaperonin antibody.** The immunoprecipitation experiment was performed using anti-TkCPN antibodies as for the following samples and analyzed by SDS-PAGE: PhCPN (*lane 1*), PhCPN and denatured GFP (*lane 2*), PhPFD, denatured GFP, and PhCPN (*lane 3*), PhPFD, 15-fold amount of denatured GFP and PhCPN (*lane 4*), PhPFD and PhCPN (*lane 5*), and PhPFD (*lane 6*). The concentrations of PhCPN, GFP, and PhPFD were 1.4, 7.0, and 7.0 μM, respectively (molar ratios, PhCPN: GFP:PhPFD = 1:5:5). The concentration of GFP was 21.0 μM in *lane 4*. The proteins were mixed and incubated at 65 °C for 10 min with the components mentioned above. For *lane 3* and *4*, PhPFD and GFP were mixed and incubated at 65 °C for 10 min prior to the addition of PhCPN. GFP, CPN, and PFD are controls for GFP, PhCPN, and PhPFD. *M*, molecular standard (83, 62, 47.5, 32.5, 25, 16.5, and 6.5 kDa).

Single Molecule Observation of Prefoldin and Chaperonin Complex Formation—We next sought to confirm the interaction between the archaeal prefoldin and a chaperonin by directly observing their association at the level of a single molecule. The α chaperonin from *Thermococcus* sp. strain KS-1 (TkCPN) was used in this experiment, because we previously determined its crystal structure (15), which enabled us to select an appropriate position for labeling with a fluorescent dye (Alexa488). Equimolar amounts (100 nM) of fluorescently labeled TkCPN (488-TkCPN) and Cy5-labeled PhPFD (Cy5-PhPFD) were incubated at 60 °C, where both protein complexes are stable, and their individual signals were observed on a slide glass using a total internal reflection fluorescence microscopy (TIRFM) system (30) (Fig. 2). The location of TkCPN was identified by the fluorescence of Alexa488 and that of PhPFD by the fluorescence of Cy5, respectively. Approximately 30% of the Alexa488 spots were found to be superimposed on Cy5 spots, directly indicating that a significant fraction of the two chaperones formed binary complexes in the absence of substrate. Our findings indicate that, as with the eukaryotic prefoldin-chaperonin system (24, 32), the archaeal counterparts likely cooperate through direct interactions to facilitate the folding of non-native polypeptides.

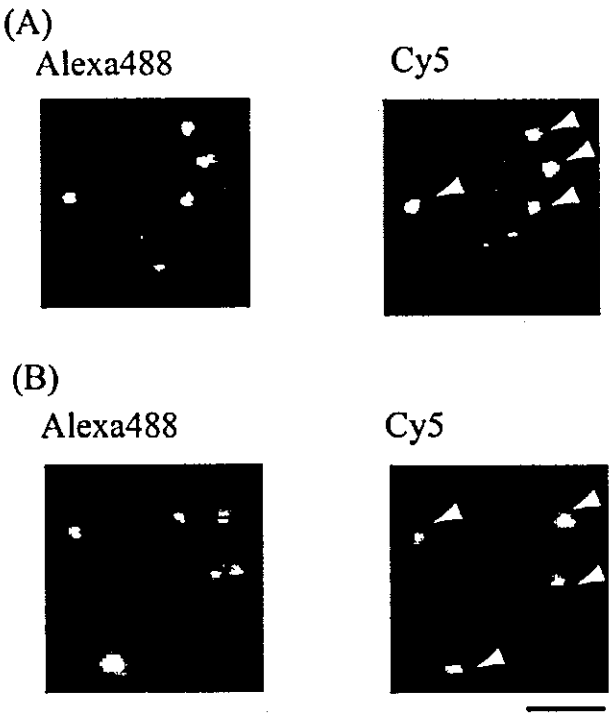

FIG. 2. **Fluorescence micrographs of the complexes between 488-TkCPN and Cy5-PhPFD.** Both *upper* and *lower panels* (*A* and *B*) were obtained from the same field. 488-TkCPNs are observed in the *left panels* (Alexa488 fluorescence), and Cy5-PhPFD are also identified in the *right panels* (Cy5 fluorescence). The co-incident spots, which represent the prefoldin-chaperonin complexes, are marked by the *arrows* in the *right panels*. The final concentrations of 488-TkCpn and Cy5-PhPFD were both 1 nM. The *scale bar* represents 5 μm.

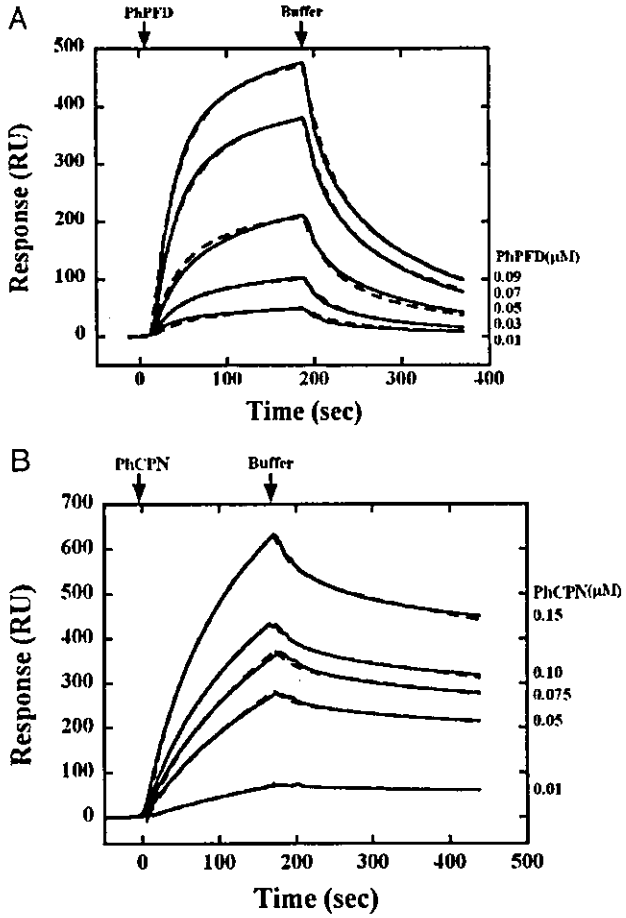

FIG. 3. **Sensorgrams of affinity measurements between PhCPN and PhPFD by surface plasmon resonance spectroscopy.** *A*, PhCPN was immobilized on a Biacore biosensor chip to be 19,000 RU, and PhPFD at 0.01, 0.03, 0.05, 0.07, and 0.09 μM were injected as the analytes. *B*, PhPFD was immobilized on a Biacore biosensor chip to be 4,500 RU, and 0.025, 0.05, 0.10, 0.15, and 0.25 μM PhCPN were injected as the analytes. Sensorgrams with different concentrations of prefoldin and fitting to the bivalent analyte model are indicated by *solid* and *dotted lines*, respectively.

Surface Plasmon Resonance of the Binding of PhPFD and PhCPN—To assess the interaction kinetics between the archaeal prefoldin and a chaperonin, we monitored their binding and release by surface plasmon resonance using a Biacore system. When PhCPN was immobilized on the sensor chip, PhPFD produced a concentration-dependent signal (Fig. 3*A*). The interaction was found to be reversible, because the signal returned to a base level ~200 s after the removal of PhPFD. When PhPFD was immobilized, the signal also augmented when an increasing concentration of PhCPN was added to the mobile phase (Fig. 3*B*). The release of PhCPN was slow, however, and a considerable amount of PhCPN remained on the sensor chip even 200 s after the wash with buffer (Fig. 3*B*).

The binding curves were fitted using various models using the BIAevaluation 3.1 software; when either PhPFD or PhCPN were immobilized on the sensor, the best fits were obtained with the bivalent analyte model (Fig. 3, *A* and *B*). Global fittings of the data using the bivalent model yielded χd values of 23.3 for immobilized PhCPN and 6.99 for immobilized PhPFD, respectively, which were optimal compared with all other tested models. Apparent association and dissociation rate constants obtained from the fitted data models are shown in Table I. The rate constants for the first step ($L + A \leftrightarrow L \cdot A$) for both experiments using PhPFD and PhCPN immobilized sensor chips are close to each other, but not identical. The discrepancy may be explained at least in part by the difference between the fitted model and real interaction mechanism and requires further investigation to obtain the actual kinetic constants for the interaction between PhPFD and PhCPN. The dissociation constant (K_D), obtained using the data from immobilized PhCPN, was calculated to be 26.4 nM by the resonance unit at equilibrium. Although the conditions of binding may not reflect the proper physiological environment in which the interaction takes place (*e.g.* temperature among other factors), the value for the dissociation constant is suggestive of a particularly tight association between the two chaperones. This tight interaction is consistent with our above immunoprecipitation and single molecule observation results.

TABLE I
Association and dissociation rate constants between PhCPN and PhPFD obtained by SPR

Ligand	PhCPN	PhPFD
k_{on1} (M^{-1}, s^{-1})	5.39×10^4	1.58×10^4
k_{off1} (s^{-1})	2.74×10^{-2}	2.23×10^{-2}
k_{on2} (RU^{-1}, s^{-1})	5.4×10^{-6}	1.18×10^{-5}
$k_{off}2$ (s^{-1})	3.47×10^{-3}	6.41×10^{-4}

Species-specific Interaction between Archaeal Chaperonin and Prefoldin—To evaluate whether the interaction between an archaeal prefoldin and a chaperonin demonstrates specificity, we compared by surface plasmon resonance the affinities of PhPFD to two other chaperonins. Compared with PhCPN, the affinity of the archaeal chaperonin TkCPN was found to be ~10-fold reduced. In addition, a group I chaperonin from *Thermus thermophilus* HB8 exhibited little or no detectable interaction with PhPFD (Fig. 4*A*). Importantly, the affinity of Mt-

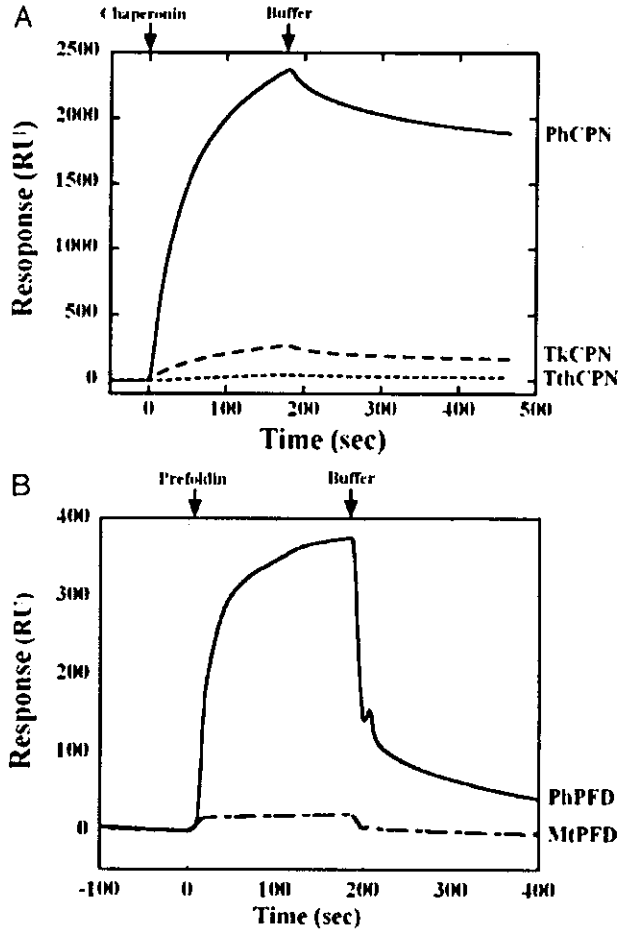

FIG. 4. **Comparison of the interaction between prefoldin and chaperonin from different sources.** *A*, PhPFD was immobilized on a Biacore biosensor chip to be 10,736 RU, and PhCPN, TkCPN, and TthCPN at 0.05 μM were injected as the analytes. *B*, PhCPN was immobilized on a Biacore biosensor chip at 9000 RU, and PhPFD and MtPFD at 0.5 μM were injected as the analytes.

PFD for PhCPN was also found to be highly reduced compared with that of PhPFD for the same chaperonin (Fig. 4*B*). Together, these data validate our above finding of a *bona fide*, specific interaction between PhPFD and PhCPN and suggest that the chaperone interactions are species-specific.

The Substrate Binding Site of the Prefoldin Is Located at the Distal Ends of the Coiled-coils—The unique jellyfish-like structure of prefoldin suggests that this chaperone can encapsulate substrates within a rectangular cavity defined by its lengthy coiled-coils (Fig. 5*A*) (23). Indeed, large truncations of the distal regions of both eukaryotic and archaeal prefoldin subunits severely affect the abilities of the mutated hexameric complexes to interact with non-native proteins (24, 25). Moreover, unfolded actin has been visualized by electron microscopy to occlude the entrance of the eukaryotic prefoldin cavity (24). However, it is unclear where the precise substrate binding site exists in either archaeal or eukaryotic prefoldin. To shed light on this question, we prepared a variety of truncated PhPFD subunits and tested their chaperone activity by measuring their ability to prevent the aggregation of heat-denatured citrate synthase (CS) and to inhibit the spontaneous refolding of acid-denatured green fluorescent protein (GFP), as previously described (26). Wild-type PhPFD efficiently protects CS from thermal aggregation (Fig. 5*B*) and prevents the renaturation of GFP (Fig. 5*C*). A hexameric PhPFD complex containing β subunits with a 5- or 6-amino acid truncation from the C terminus (tc5β or tc6β, respectively) had almost the same ability to interact with the two non-native substrates as the wild-type (Table II). The effect of an 8-amino acid truncation from the C termini of the α and β subunits (tc8α and tc8β, respectively) were then examined (Fig. 5). The PhPFD complex containing mutant β subunit (tc8β) failed to efficiently suppress the thermal aggregation of CS and had little ability to prevent GFP refolding (Fig. 5, *B* and *C*). On the other hand, the truncated α subunit showed no observable effect on CS aggregation or GFP refolding (Fig. 5, *B* and *C*). Given that the removal of 5 or 6 residues from the C terminus of the PhPFD β subunit had little effect but deletion of 8 residues had a considerable effect on the chaperone activity of the complex, we conclude that Leu^{111} and Ala^{110} of the last 8 amino acids (Ala^{110}-Leu^{111}-Arg^{112}-Pro^{113}-Pro^{114}-Thr^{115}-Ala^{116}-Gly^{117}-COOH) are important for chaperone-substrate interactions. Consistent with this result, amino acid replacement of Leu^{111} to Ala partially affects substrate binding (Table II). Importantly, residues from the N terminus of the β subunit were also found to be important for substrate binding as a prefoldin complex containing a 10-residue truncation in the β subunit (wtαtn10β) was found to have compromised chaperone activity (Table II).

The contribution of the α subunit to chaperone activity was found to be important but somewhat less critical. The 8-amino acid C-terminal truncation of α subunit (tc8α) had almost no effect on the molecular chaperone activities of the PhPFD complexes with wild or truncated β subunits. However, a complex containing a 17-amino acid N-terminal truncation from the α subunit (tn17α) affected the ability of prefoldin to prevent the aggregation of CS, while not having an observable effect on GFP refolding.

Effects of PhPFD Truncations on the Interaction with PhCPN—From a recent electron microscopy image of eukaryotic prefoldin bound to the CCT chaperonin, presently unidentified distal regions within (one or more) "tentacles" of prefoldin are likely to contact the chaperonin cylinder (24). The recombinant subunits bearing truncations therefore allowed us to test which of the one or more regions within the coiled-coils of archaeal prefoldin interact with the chaperonin. We examined the interaction of the truncated mutants with PhCPN by surface plasmon resonance (SPR) using the chaperonin-bound sensor chip. A PhPFD complex lacking 8 C-terminal residues within the α subunit (tc8αwtβ) exhibited almost the same binding response as that of the wild-type complex (Fig. 6*A*). Importantly, analysis of a prefoldin complex lacking 8 C-terminal residues in the β subunit revealed that this distal end region was critical for the interaction with PhCPN (Fig. 6, *B* and *C*).

Dissociation constants (K_D) between PhPFD mutants and PhCPN were calculated by the resonance unit at equilibrium. The K_D values of the various mutant PhPFD complexes are represented in Table III in relation to the K_D values of wild-type PhPFD. Interestingly, the relative K_D values were found to increase in a stepwise manner with the removal of 5 to 7 C-terminal residues in the β subunit (Table III). A mutant complex, wtαtc5β, has nearly the same affinity for PhCPN, but that of wtαtc7β is decreased ~10-fold. Remarkably, the residue Leu^{111} was found to be critical for the interaction of PhPFD with PhCPN, because its mutagenesis to alanine resulted in a similar decrease of affinity compared with the deletion of 8 C-terminal amino acids. The N-terminal region of the β subunit was also found to be important for chaperonin interactions, because a 10-amino acid deletion (wtαtn10β) showed substantially reduced binding to the chaperonin (15-fold higher relative K_D). On the other hand, a prefoldin complex containing the wild-type β subunit and 8- or 17-amino acid truncation in the C- or N-terminal

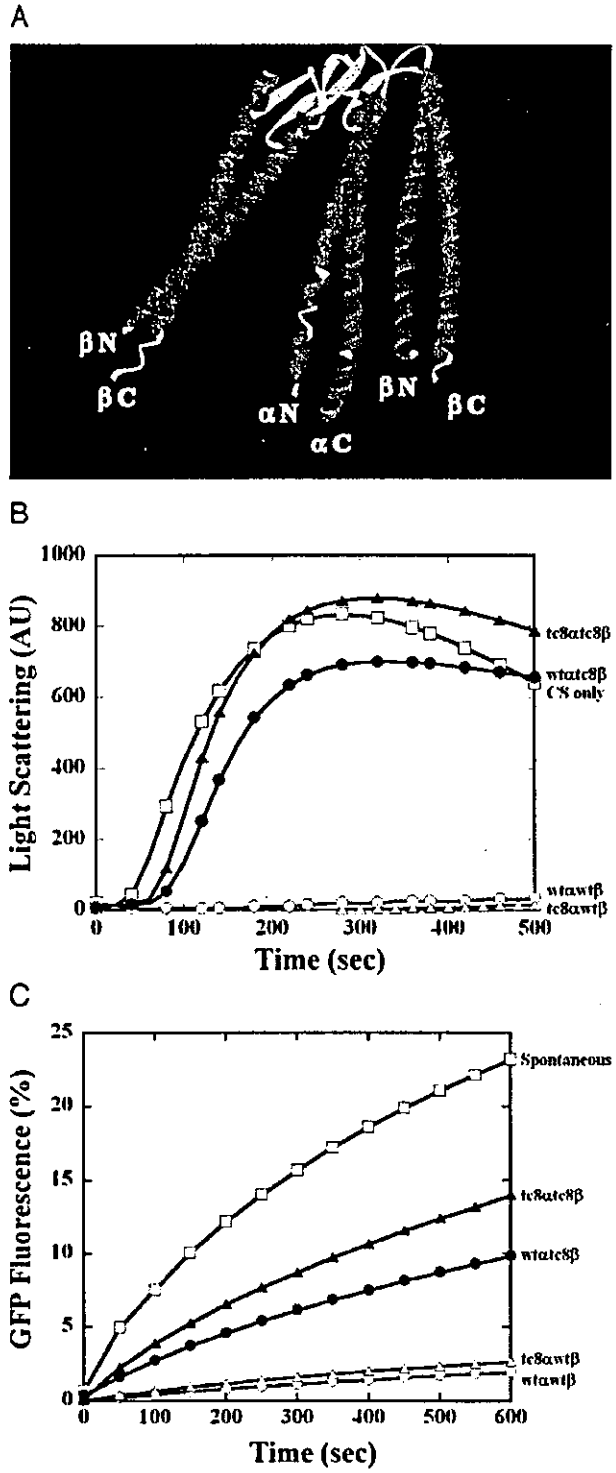

FIG. 5. **Effects of 8-amino acid truncations from the C terminus of prefoldin subunits on their activities for the protection of CS from thermal aggregation and arresting spontaneous refolding of GFP.** *A*, structure of prefoldin (asymmetric unit). N and C termini of α and β subunits are designated as *Nα*, *Cα*, *Nβ*, and *Cβ*, respectively. The coordinates are from the Protein Data Bank code 1FXK (23), and the figures were drawn with Viewer Light (Accelrys). *B*, thermal aggregation of CS from porcine heart was monitored by measuring the light scattering at 500 nm with a spectrofluorophotometer at 50 °C with continuous stirring. Monitoring started with the addition of CS (80 nM as a monomer) to 50 mM Tris-HCl buffer (pH 8.0) preincubated at 50 °C without (*open square*) or with 240 nM wild-type PhPFD (*open circle*), wtαtc8β (*close circle*), tc8αwtβ (*open triangle*), or tc8αtc8β (*close triangle*). *C*, GFP folding was monitored by the fluorescence at 510 nm with excitation at 396 nm using a spectrofluorophotometer. GFP was denatured in 12.5 mM HCl. The fluorescence measurement was started with addition of 15 μM native or denatured GFP (10 μl) into 1.5 ml of dilution buffer (50 mM Tris-HCl, pH 8.0, 100 mM KCl, 5 mM dithiothreitol, and 25 mM $MgCl_2$) and was preincubated at 60 °C and under continuous stirring without PhPFD (*open square*) or with 500 nM of wild-type PhPFD (*open circle*), wtαtc8β (*close circle*), tc8αwtβ (*open triangle*), or tc8αtc8β (*close triangle*) at a molar ratio of 1:5 (denatured GFP:prefoldin).

TABLE II

Relative activities of mutated PhPFDs for the protection of CS from thermal aggregation and arrest of GFP spontaneous refolding

Refolding of acid-denatured GFP in the presence or absence of PhPFD derivatives at a molar ratio of 1:5 was monitored by the fluorescence at 510 nm with excitation at 396 nm using a spectrofluorophotometer. Relative suppression of fluorescence recovery at 500 s against wild-type was calculated. Thermal aggregation of CS in the presence or absence of PhPFD derivatives at a molar ratio of 1:5 was monitored by measuring the light scattering at 500 nm with a spectrofluorophotometer at 50 °C. Relative suppression of CS aggregation at 200 s against wild-type was calculated.

PhPFD		GFP, relative suppression of spontaneous refolding	CS, relative suppression of thermal aggregation
α subunit	β subunit		
		%	%
wtα	wtβ	100	100
wtα	tc5β	102	99
wtα	tc6β	101	100
wtα	tc7β	66	101
wtα	tc8β	63	24
wtα	L111Aβ	35	92
tc8α	Wtβ	97	102
tc8α	tc5β	102	100
tc8α	tc6β	90	100
tc8α	tc7β	65	100
tc8α	tc8β	43	0
tc8α	L111Aβ	99	95
wt α	Tn10β	26	78
tn17α	wtβ	85	46
tn17α	Tn10β	38	55

regions of the α subunit (tc8αwtβ and tn17αwtβ, respectively) had little effect on its interaction with chaperonin. Given the possible co-axial binding of multiple prefoldin tentacles to the apical regions of the chaperonin toroid (24), we tested the effect of combined α and β subunit truncations on chaperonin binding. Truncations of the β subunit in the tc8α background, *i.e.* tc8αtc(5, 6, 7 or 8)β, revealed an additive loss of affinity for the chaperonin when compared with the tc8α mutant subunit by itself (Table III). These data strongly suggest that both subunits bind the chaperonin cooperatively.

DISCUSSION

In this study, we have studied the interaction between the prefoldin and a chaperonin from hyperthermophilic archaea by immunoprecipitation, single molecule observation, and SPR. We observed complex formation between PhPFD and PhCPN by immunoprecipitation with anti-TkCPN antibody (Fig. 1). In the single molecule observation using TIRFM, a significant number of chaperonin molecules made complexes with prefoldin molecules (Fig. 2). Both *M. thermoautotrophicum* and *P. horikoshii* archaeal prefoldin complexes can stabilize non-native proteins and transfer them to a chaperonin for folding to the native state (22, 26). *In vivo*, the interaction with the chaperonin may therefore facilitate the specific and efficient handover of an aggregation-prone polypeptide to a chaperonin in such a manner as to prevent inappropriate interactions with cellular components.

The kinetics of the reaction between prefoldin and chaperonin was studied using SPR. Simulated curves of the bivalent analyte model were best fit to the experimental curves (Fig. 3,

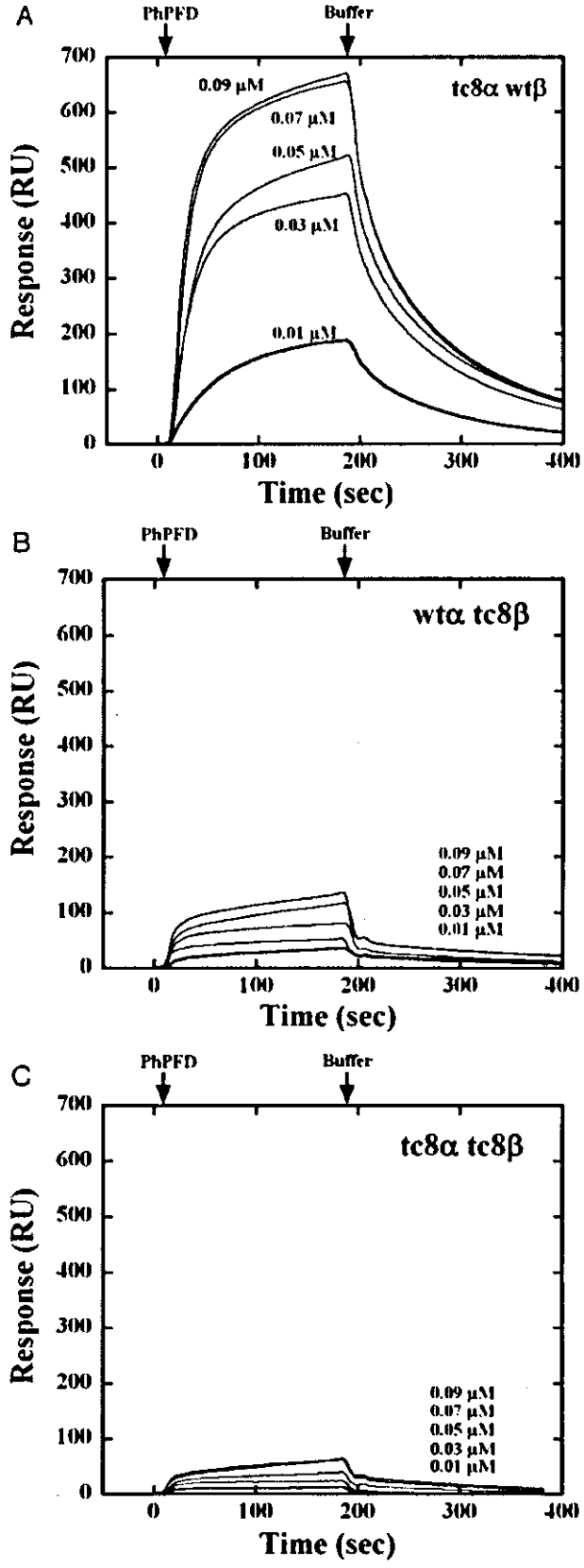

FIG. 6. **Effects of mutations in PhPFDs on the interaction with PhCPN.** PhCPN was immobilized on a Biacore biosensor chip and PhPFDs (tc8αwtβ (*A*), wtαtc8β (*B*), or tc8αc8β (C)) at 0.01, 0.03, 0.05, 0.07, and 0.09 μM were injected as the analytes.

TABLE III

K_D values for the interaction between the mutant PhPFDs and PhCPN

K_D values were calculated by the resonance unit at the equilibrium. Relative K_D values were calculated by dividing the K_D values by that of the wild-type PhPFD.

PhPFD		K_D	Relative K_D
α subunit	β subunit		
		10^{-8} M	
Wtα	wtβ	2.63	
Wtα	tc5β	4.59	1.74
Wtα	tc6β	11.0	4.18
Wtα	tc7β	28.8	11.0
Wtα	tc8β	30.8	11.7
Wtα	L117Aβ	42.9	16.3
Tc8α	wtβ	2.13	0.81
Tc8α	tc5β	35.5	13.5
Tc8α	tc6β	26.0	9.89
Tc8α	tc7β	57.7	21.9
Tc8α	tc8β	69.3	26.3
Tc8α	L117Aβ	84.9	32.2
Wtα	tn10β	44.7	17.0
tn17α	wtβ	2.03	0.77
tn17α	tn10β	18.1	6.88

A and *B*). It is thought that prefoldin and chaperonin interact through six coiled-coils of prefoldin and eight apical domains of the chaperonin. Thus, it is reasonable that the interaction is most optimally fitted by the multivalent model. The kinetic constants calculated from the sensorgrams with PhCPN- and PhPFD-immobilized sensor chips are different. It might be partly due to the irreversibility of the sensorgram obtained with the PhPFD-immobilized chip, which is likely to be caused by the binding of PhCPN to multiple PhPFDs on a chip.

In this study, we obtained evidence for a species-specific interaction between prefoldin and its cognate chaperonin. Despite the high sequence homology between TkCPN and PhCPN, their affinities for PhPFD were considerably different. Although we demonstrated cooperation between PhPFD and TthCPN in the previous paper, we could not observe significant interaction between PhPFD and TthCPN by SPR. Recently, we have found that the binding between PhPFD and substrate is in dynamic equilibrium.[3] Thus, it might be that the substrate was not directly transferred to TthCPN, but that protein released from PhPFD was captured by TthCPN.

Both N- and C-terminal ends of β subunit are critical for interaction with unfolded proteins and chaperonins. In particular, the binding site in the C-terminal region was localized to the C-terminal 8 amino acid residues of β subunit (Ala^{110}-Leu^{111}-Arg^{112}-Pro^{113}-Pro^{114}-Thr^{115}-Ala^{116}-Gly^{117}-COOH). Specifically, Ala^{110} and Leu^{111} appear to be essential for the interaction of prefoldin with unfolded proteins. Although we show that the hydrophobicity of Leu^{111} is important for the interaction, its contribution is only marginal (Table II). For the interaction with PhCPN, K_D gradually increased with the deletion from 5 to 7 amino acids. Thus, the binding site for the chaperonin is adjacent to that of an unfolded protein, which may correlate with the effective handover of an aggregation-prone polypeptide to a chaperonin. The main difference between substrate recognition and chaperonin binding is the lowered affinity for chaperonin of tc8αtc5β, which exhibits almost same affinities for CS and GFP as that of the wild-type. We have observed acceleration of release of substrate from the prefoldin by chaperonins.[3] The effect was not observed for the mutant PhPFD complex, tc8αtc5βt, which correlates with the decrease of the affinity with the chaperonin. Therefore, there is likely to be cooperation between α and β subunits in the interaction

[3] T. Zako, R. Iizuka, M. Okochi, T. Ueno, H. Tadakuma, M. Yohda, and T. Funatsu, manuscript in preparation.

with a chaperonin, which is important for the substrate handover to the chaperonin.

A ternary complex of the prefoldin, a chaperonin, and a substrate protein should occur transiently during the substrate handover from the prefoldin and chaperonin. Thus, it is reasonable that the interaction between the prefoldin and the chaperonin is affected by the presence of a substrate protein. Contrary to our expectation, almost no significant difference was observed in the immunoprecipitation experiment between the presence and absence of denatured proteins (Fig. 1). To elucidate substrate handover mechanism, the affect of a substrate protein on the kinetics for the interaction between the prefoldin and chaperonin should be examined in more detail.

Acknowledgments—We thank V. F. Lundin and P. C. Stirling for preparation of MtPFD. We appreciate Kaori Morimoto for support in the analysis of kinetic constants.

REFERENCES

1. Gething, M. J., and Sambrook, J. (1992) *Nature* **355**, 33–45
2. Ellis, R. J., and Hartl, F. U. (1996) *FASEB J.* **10**, 20–26
3. Bukau, B., and Horwich, A. L. (1998) *Cell* **92**, 351–366
4. Ranson, N. A., White, H. E., and Saibil, H. R. (1998) *Biochem. J.* **333**, 233–242
5. Yoshida, T., Kawaguchi, R., Taguchi, H., Yoshida, M., Yasunaga, T., Wakabayashi, T., Yohda, M., and Maruyama, T. (2002) *J. Mol. Biol.* **315**, 73–85
6. Kim, S., Willison, K. R., and Horwich, A. L. (1994) *Trends Biochem. Sci.* **19**, 543–548
7. Kubota, H., Hynes, G., and Willison, K. (1995) *Eur. J. Biochem.* **230**, 3–16
8. Hartl, F. U. (1996) *Nature* **381**, 571–579
9. Fenton, W. A., and Horwich, A. L. (1997) *Protein Sci.* **6**, 743–760
10. Sigler, P. B., Xu, Z., Rye, H. S., Burston, S. G., Fenton, W. A., and Horwich, A. L. (1998) *Annu. Rev. Biochem.* **67**, 581–608
11. Archibald, J. M., Logsdon, J. M., and Doolittle, W. F. (1999) *Curr. Biol.* **9**, 1053–1056
12. Gutsche, I., Essen, L. O., and Baumeister, W. (1999) *J. Mol. Biol.* **293**, 295–312
13. Klumpp, M., Baumeister, W., and Essen, L. O. (1997) *Cell* **91**, 263–270
14. Ditzel, L., Lowe, J., Stock, D., Stetter, K. O., Huber, H., Huber, R., and Steinbacher, S. (1998) *Cell* **93**, 125–138
15. Shomura, Y., Yoshida, T., Iizuka, R., Maruyama, T., Yohda, M., and Miki, K. (2004) *J. Mol. Biol.* **335**, 1265–1278
16. Gutsche, I., Holzinger, J., Rauh, N., Baumeister, W., and May, R. P. (2001) *J. Struct. Biol.* **135**, 139–146
17. Iizuka, R., Yoshida, T., Shomura, Y., Miki, K., Maruyama, T., Odaka, M., and Yohda, M. (2003) *J. Biol. Chem.* **278**, 44959–44965
18. Meyer, A. S., Gillespie, J. R., Walther, D., Millet, I. S., Doniach, S., and Frydman, J. (2003) *Cell* **113**, 369–381
19. Geissler, S., Siegers, K., and Schiebel, E. (1998) *EMBO J.* **17**, 952–966
20. Hansen, W. J., Cowan, N. J., and Welch, W. J. (1999) *J. Cell Biol.* **145**, 265–277
21. Vainberg, I. E., Lewis, S. A., Rommelaere, H., Ampe, C., Vandekerckhove, J., Klein, H. L., and Cowan, N. J. (1998) *Cell* **93**, 863–873
22. Leroux, M. R., Fandrich, M., Klunker, D., Siegers, K., Lupas, A. N., Brown, J. R., Schiebel, E., Dobson, C. M., and Hartl, F. U. (1999) *EMBO J.* **18**, 6730–6743
23. Siegert, R., Leroux, M. R., Scheufler, C., Hartl, F. U., and Moarefi, I. (2000) *Cell* **103**, 621–632
24. Martin-Benito, J., Boskovic, J., Gomez-Puertas, P., Carrascosa, J. L., Simons, C. T., Lewis, S. A., Bartolini, F., Cowan, N. J., and Valpuesta, J. M. (2002) *EMBO J.* **21**, 6377–6386
25. Simons, C. T., Staes, A., Rommelaere, H., Ampe, C., Lewis, S. A., and Cowan, N. J. (2004) *J. Biol. Chem.* **279**, 4196–4203
26. Okochi, M., Yoshida, T., Maruyama, T., Kawarabayasi, Y., Kikuchi, H., and Yohda, M. (2002) *Biochem. Biophys. Res. Commun.* **291**, 769–774
27. Sakikawa, C., Taguchi, H., Makino, Y., and Yoshida, M. (1999) *J. Biol. Chem.* **274**, 21251–21256
28. Iizuka, R., Yoshida, T., Maruyama, T., Shomura, Y., Miki, K., and Yohda, M. (2001) *Biochem. Biophys. Res. Commun.* **289**, 1118–1124
29. Yoshida, T., Ideno, A., Hiyamuta, S., Yohda, M., and Maruyama, T. (2001) *Mol. Microbiol.* **39**, 1406–1413
30. Funatsu, T., Harada, Y., Tokunaga, M., Saito, K., and Yanagida, T. (1995) *Nature* **374**, 555–559
31. Bradford, M. M. (1976) *Anal. Biochem.* **72**, 248–254
32. Siegers, K., Waldmann, T., Leroux, M. R., Grein, K., Shevchenko, A., Schiebel, E., and Hartl, F. U. (1999) *EMBO J.* **18**, 75–84

Available online at www.sciencedirect.com

SCIENCE DIRECT

Thin Solid Films 464–465 (2004) 452–455

www.elsevier.com/locate/tsf

Attachment of DNA to microfabricated arrays with self-assembled monolayer

Guo-Jun Zhang[a,*], Takashi Tanii[b], Takeo Miyake[b], Takashi Funatsu[a,c], Iwao Ohdomari[a,b,d]

[a] *Nanotechnology Research Center, Waseda University, Waseda Tsurumaki-cho 513, Shinjuku, Tokyo 162-0041, Japan*
[b] *Department of Electronical Engineering and Bioscience, Waseda University, 3-4-1 Okubo, Shinjuku, Tokyo 169-8555, Japan*
[c] *Department of Physics, School of Science and Engineering, Waseda University, 3-4-1 Okubo, Shinjuku, Tokyo 169-8555, Japan*
[d] *Kagami Memorial Laboratory for Materials Science and Technology, Waseda University, 2-8-26 Nishi-waseda, Shinjuku, Tokyo 169-0051, Japan*

Available online 17 July 2004

Abstract

A novel approach of fabricating sub-10-μm patterns on silicon surfaces by electron beam (EB) lithography for attachment of oligonucleotides was described. The shape of the microfabricated arrays was observed to be regular by optical microscopy. An octadecyltrimethoxysilane (ODS) monolayer was deposited on the regions outside the patterned areas to minimize the nonspecific binding of biomolecules. Cy 5-labeled target DNA was hybridized to both complementary and noncomplementary oligonucleotides that were covalently anchored to micropatterns. As a result, the micropatterns where specific binding occurred show strong signals, whereas no signals are observed in the case of nonspecific binding. These data indicate that miniature micro- and nano-arrays will find applications in biochips and biosensors.

PACS: 85.40.Hp Lithography, masks and pattern transfer; 87.14. Gg DNA, RNA; 82.40.Np Temporal and spatial patterns in surface reactions; 81.16. Dn Self-assembly
Keywords: Electron beam lithography; Fabrication; Micropatterns; DNA; Attachment; Fluorescence detection

1. Introduction

DNA microarrays have extensively been applied to the development of techniques for disease diagnosis, drug discovery, DNA sequencing, and gene expression [1,2]. There are two main approaches to creating DNA arrays on glass surfaces. One approach is to utilize a photolithography technique to position DNA oligonucleotides on the arrays [3]. Using this method, oligonucleotides are synthesized directly on the arrays by numerous cycles of photodeprotection and sequential masks. Another approach is to attach presynthesized DNA probes onto designated areas on a solid substrate [4]. In this approach, presynthesized oligonucleotides are patterned onto a chemically active surface and immobilized by introducing functional groups. Many different types of materials have been used as substrates for DNA attachment including glass slides [5,6], gold [7,8], silicon [9–12], and diamond [13,14]. Among these materials, silicon wafers have less surface roughness, resulting in the uniform deposition of short DNAs at a high density with the development of high-resolution lithography techniques [15]. Therefore, it is important to explore the potential of miniaturizing DNA arrays with a high density of biochip elements and small amounts of reaction reagents on the silicon surface.

Compared with conventional microarray technology, the fabrication of microarrays using EB lithography can allow us to precisely deposit biomolecules (DNA/protein) on a substrate and yield controlled homogeneous spots, resulting in high detection sensitivity and massive parallelization. In our previous study, we demonstrate that micropatterns can be fabricated on a resist on silicon surfaces by EB lithography for DNA immobilization [16]. In the protocol, after EB lithography, the patterns are activated and modified with 3-aminopropyltriethoxysilane (APTES) to generate amino groups. After the resist film is completely removed, amino-terminated patterns are obtained on silicon surfaces. These patterns are then functionalized with oligonucleotides. However, APTES is a small molecule and does not form an oriented self-assembled monolayer rather, it forms a multilayer packed within the amino-modified patterns. After the removal of the resist, some APTES molecules on the top of

* Corresponding author. Tel.: +81-3-5286-9067; fax: +81-3-5286-9076.
E-mail address: zhang@kaw.comm.waseda.ac.jp (G.-J. Zhang).

0040-6090/$ - see front matter © 2004 Elsevier B.V. All rights reserved.
doi:10.1016/j.tsf.2004.06.057

the multilayer occupy areas where resist exists, thereby leading to irregular fluorescence patterns. Thus, it is difficult to fabricate smaller arrays by this method.

In this paper, we present an alternative method of fabricating sub-10-μm patterns on silicon substrates by EB lithography for attachment of oligonucleotides. The resist micropatterns were fabricated by EB lithography. An octadecyltrimethoxysilane (ODS) monolayer was deposited on the surface after the fabrication of the resist patterns. The amino groups were introduced to the resist-patterned areas after the resist was removed. Oligonucleotides were covalently attached to amino-modified micropatterns using crosslinker molecules. Fluorescence signals were obtained to determine hybridization specificity by epi-fluorescence microscopy. The resulting fluorescence patterns indicate that DNA microarrays fabricated by this method show more precise control over pattern size, shape, and pitch than those fabricated by our previous method [16]. More importantly, using this protocol, DNA nano-arrays have also been observed, which is more effective than the previous method.

2. Experimental

All the oligonucleotides used were purchased from the Sigma Genosys Japan (Hokkaido, Japan). The complementary and noncomplementary oligonucleotides used for immobilization were amino-modified at the 5′ end, and oligonucleotides employed for hybridization to the surface were Cy 5-labeled at the 5′ end. Each of these oligonucleotides was 21 mer in length. The three 21-mer sequences employed were

H2N-5′-CCACGGACTACTTCAAAACTA-3′-(complementary),
H2N-5′-ATCGATCGATCGATCGATCGA-3′(non-complementary),
Cy 5-5′-TAGTTTTGAAGTAGTCCGTGG-3′(target).

All the chemicals and solvents used were purchased from Kanto Chemical (Tokyo, Japan) except APTES, ODS, and ethyltriethoxysilane which were from Acros (USA), and the resist and remover which were from Shipley (USA). The wafers used for the experiments were n-type Si (100) wafers. Ultrapure water was obtained from a Millipore system.

2.1. Microfabrication by EB lithography

A resist film was coated on a SiO_2 layer as described previously [16]. The resist micropatterns were fabricated with a 20-KeV focused electron beam (EB) using the Hitachi-modified S-4200 electron beam lithography system.

2.2. Chemical vapor deposition (CVD)

After the patterning, the surface was activated by treatment with a mixture of ammonium hydroxide/hydrogen peroxide/water, and an ODS monolayer was deposited on the substrates at 110 °C for 3 h in N_2 atmosphere by chemical vapor deposition (CVD). The surface was then washed with chloroform for 10 min by ultrasonication. The substrate was immersed in a solution of 1 mM ethyltriethoxysilane (ETS) in ethanol for 1 h and washed with ethanol by ultrasonication. The hydrophobic ODS monolayer prevented the unspecific binding of biomoleclues.

2.3. Attachment of DNA to microfabricated arrays

The resist was totally removed by immersing the specimen in the remover overnight, leaving micropatterns in the ODS monolayer. Then the substrates were rinsed with acetone (1 × 5 min), ethanol (1 × 5 min), and H_2O (1 × 5 min) by ultrasonication. The micropatterns were activated by immersing them in a solution of $NH_4OH/H_2O_2/H_2O$ (1:1:4) for 5 min. The substrates were finally rinsed with H_2O and dried. The surface modification and immobilization of the 5′

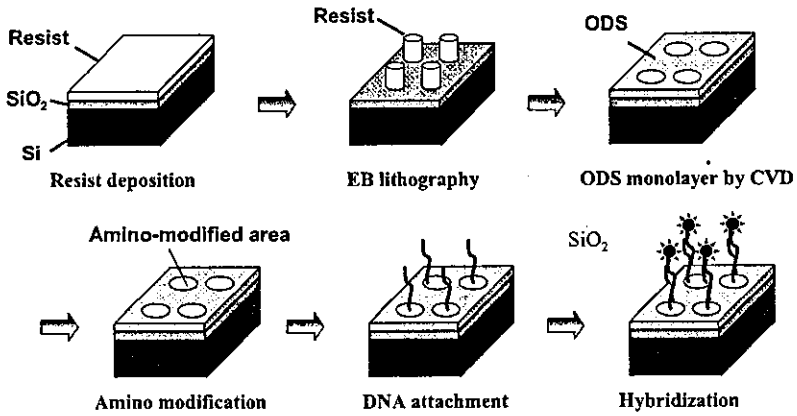

Fig. 1. Schematic diagram of attachment of oligonucleotides to micropatterns fabricated by EB lithography.

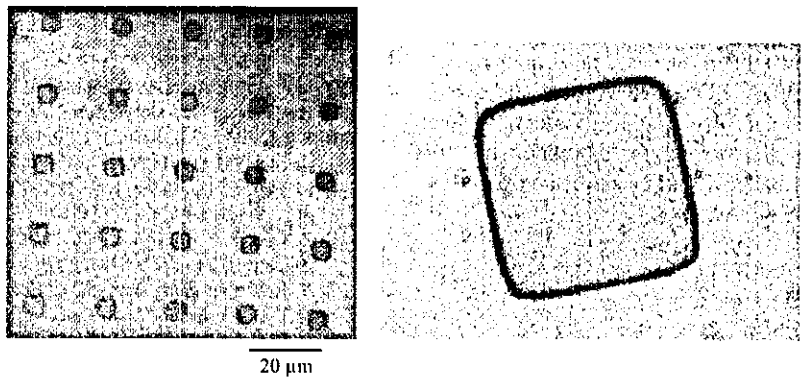

Fig. 2. Optical images of microarrays fabricated by EB lithography. (a) Overview of microarrays (diameter: 5 μm, pitch: 20μm); (b) magnified view of single dot.

amino-modified probe DNA on the micropatterns were carried out using our previous protocol [16].

2.4. Hybridization

The DNA-modified micropatterns were exposed to 1 μl of 1 μM Cy 5-labeled DNA complement in a solution of 2 × SSC and 0.2% SDS, and hybridized at 59 °C for 3 h in a humid chamber. The hybridized surfaces were then washed with 2 × SSC containing 0.2% SDS, 2 × SSC, and 0.2 × SSC, respectively. The micropatterns were finally imaged by epi-fluorescence microscopy.

3. Results and discussion

The scheme for attaching DNA onto the micropatterns by EB lithography is shown in Fig. 1. To observe the shape of the micropatterns fabricated by EB lithography, the micropatterns were imaged by optical microscopy. As shown in Fig. 2, the pattern is 5×5 μm^2 (Fig. 2b), and the pitch between two patterns is 20 μm (Fig. 2a). The shape of each individual micropattern is regular and the corresponding arrays are uniform. The images obtained indicate that microfabrication based on EB lithography can be achieved with a well-ordered array, pointing to the possible production of nanopatterns using this technique.

Sequence specificity was examined with an epi-fluorescence microscopy by applying Cy 5-labeled target DNA to the immobilized probe DNA within micropatterns. The Cy 5-labeled target DNA was hybridized to the micropatterns immobilized with complementary and noncomplementary sequences. The resulting fluorescence images show that the unspecific binding of the noncomplementary probe to the target DNA labeled with Cy 5 yielded no signals (Fig. 3b). However, sufficiently bright fluorescence patterns have been observed, indicating that hybridization occurred due to the specific binding of the probe complementary to the target (Fig. 3a). Clearly, the fluorescent micropatterns are homogenous in size and shape, corresponding to the micopatterns imaged by optical microscopy. These results indicate that the micropatterns are covalently immobilized with the probe DNA, hybridization specifically occurs due to DNA–DNA interactions, and controlled uniform spots are achieved by our method.

Furthermore, sequence-specific binding likewise leads to strong fluorescent signals visualized within nanofabricated patterns (Fig. 3c). As shown in Fig. 3c, the diameter of individual spot is 500 nm, and the pitch between two spots is 5 μm. However, Fig. 3c shows a slightly stronger background than Fig. 3a, likely because much fewer probe molecules are assembled within a 500-nm-size spot and a much lower signal-to-noise ratio is obtained than that in the case of larger spots.

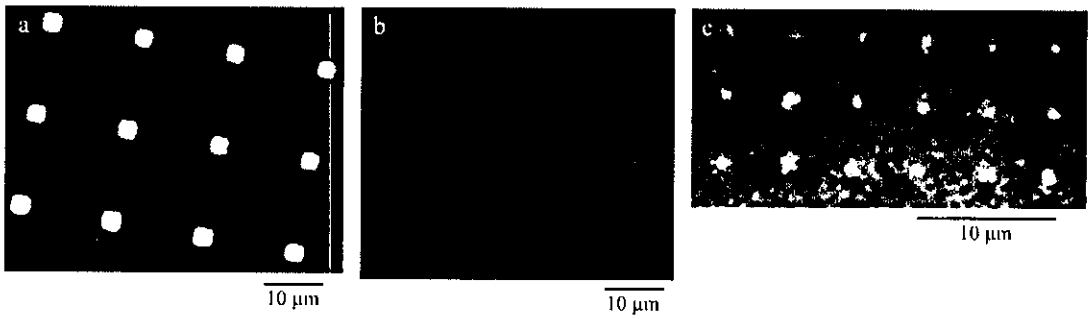

Fig. 3. Fluorescence images of hybridization of Cy 5 labeled target to probe DNA attached onto the micro- and nano-fabricated arrays. (a) Complementary probe (diameter: 5 μm, pitch: 20 μm); (b) noncomplementary probe (diameter: 5 μm, pitch: 20 μm); (c) complementary probe (diameter: 500 nm, pitch: 5 μm).

The results shown above establish the potential of high-density DNA arrays on silicon surfaces fabricated by EB lithography as a platform for DNA attachment and subsequent DNA biosensor and biochip development. We are currently miniaturizing the pattern to less than 100 nm. Smaller nanostructured patterns will be fabricated based on this technique for DNA nano-arrays.

4. Conclusion

An alternative to EB lithography for producing sub 10-μm patterns for immobilization of oligonucleotides is introduced. DNA micro- and nano-arrays were produced by covalently attaching oligonucleotides to micro- and nano-fabricated patterns. Sequence specificity was demonstrated via hybridization of a fluorescently labeled target DNA to complementary and noncomplementary probe DNAs. The resulting DNA fluorescent micropatterns were markedly uniform in size and shape, resulting in controlled homogeneous spots. This method enables the fabrication of biostructures with nanometer-scale precision, which will help advance the nanofabrication of DNA biosensors and biochips.

Acknowledgements

This work is supported in part by the Japan Society for the Promotion of Science (JSPS), and a Grant-in-Aid for Center of Excellence (COE) Research from the Ministry of Education, Culture, Sports, Science and Technology.

References

[1] M.J. Heller, Annu. Rev. Biomed. Eng. 4 (2002) 129.
[2] E.S. Lander, Nat. Genet. Suppl. 21 (1999) 3.
[3] S.P.A. Fodor, J.L. Read, M.C. Pirrung, L. Stryer, L.A. Tsai, D. Solas, Science 251 (1991) 767.
[4] M. Schena, D. Shalon, R.W. Davis, P.O. Brown, Science 270 (1995) 467.
[5] Z. Guo, R.A. Guilfoyle, A.J. Thiel, R. Wang, L.M. Smith, Nucleic Acids Res. 22 (1994) 5456.
[6] Y. Rogers, P. Jiang-Baucom, Z. Huang, V. Bogdanov, S. Anderson, M.T. Boyce-Jacino, Anal. Biochem. 266 (1999) 23.
[7] R. Levicky, T.M. Herne, M.J. Tarlov, S.K. Satija, J. Am. Chem. Soc. 120 (1998) 9787.
[8] S. Tombelli, M. Mascini, A.P.F. Turner, Biosens. Bioelectron. 17 (2002) 929.
[9] T. Strother, W. Cai, X.S. Zhao, R.J. Hamers, L.M. Smith, J. Am. Chem. Soc. 122 (2000) 1205.
[10] T. Strother, R.J. Hamers, L.M. Smith, Nucleic Acids Res. 28 (2000) 3535.
[11] R. Lenigk, M. Carles, N.Y. Ip, N.J. Sucher, Langmuir 17 (2001) 2497.
[12] L. Zhang, T. Strother, W. Cai, X.P. Cao, L.M. Smith, R.J. Hamers, Langmuir 18 (2002) 788.
[13] W.S. Yang, O. Auciello, J.E. Butler, W. Cai, J.A. Carlisle, J.E. Gerbi, D.M. Gruen, T. Knickerbocker, T.L. Lasseter, J.N. Russell, L.M. Smith, R.J. Hamers, Nat. Mater. 1 (2002) 253.
[14] G.-J. Zhang, H. Umezawa, H. Hata, T. Zako, T. Funatsu, H. Kawarada, I. Ohdomari, Micropatterning oligonucleotides on single crystal diamond surface by photolithography, Langmuir, submitted for publication.
[15] T.M. Harris, A. Massimi, G. Childs, Nat. Biotechnol. 18 (2000) 384.
[16] G.-J. Zhang, T. Tanii, T. Zako, T. Funatsu, I. Ohdomari, Sens. Actuators, B, Chem. 97 (2004) 243–248.

Available online at www.sciencedirect.com
SCIENCE DIRECT
ELSEVIER
Applied Surface Science 234 (2004) 102–106
applied surface science
www.elsevier.com/locate/apsusc

Preferential immobilization of biomolecules on silicon microstructure array by means of electron beam lithography on organosilane self-assembled monolayer resist

Takashi Tanii[a,*], Takumi Hosaka[a], Takeo Miyake[a], Guo-Jun Zhang[a], Tamotsu Zako[a], Takashi Funatsu[a,b], Iwao Ohdomari[a,b,c]

[a]*School of Science and Engineering, Waseda University, 3-4-1 Ohkubo, Shinjuku-ku, Tokyo 169-8555, Japan*
[b]*Nanotechnology Research Center, Waseda University, 513 Waseda-Tsurumaki-cho, Shinjuku-ku, Tokyo 162-0041, Japan*
[c]*Kagami Memorial Laboratory for Materials Science and Technology, Waseda University, 2-8-26 Nishi-waseda, Shinjuku-ku, Tokyo 169-0051, Japan*

Available online 19 June 2004

Abstract

A novel fabrication process of silicon microstructure array for preferential immobilization of biomolecules is proposed. We perform electron beam lithography on a self-assembled monolayer (SAM), and achieve high-density silicon patterns terminated with both 3-aminopropyltriethoxysilane (APTES) and octadecyltrimethoxysilane (ODS). The amino-terminated surface produces the site-directed covalent immobilization of DNA inside the pattern, while the hydrophobic surface of the ODS-SAM prevents the adsorption. As a result, we have succeeded in immobilizing the DNA within the amino-modified area. By using this methodology, we demonstrate the miniaturization of deoxyribonucleic acid (DNA) chip. After the covalent attachment of the amino-modified oligonucleotides to the microstructures, we hybridize the immobilized DNA with the target DNA labeled with a fluorescent dye. The signals from the DNA chip exhibit the specific binding due to the DNA–DNA interaction. These results show the feasibility of this technique for high-density information storage and biochip miniaturization.

PACS: 81.07.Nb molecular nanostructures; 81.16.Dn self-assembly; 81.16.Rf nanoscale pattern formation; 87.14.Gg DNA; RNA

Keywords: Electron beam; Lithography; EB; Self-assembled monolayer; SAM; Deoxyribonucleic acid; DNA; Immobilization; Biochip

1. Introduction

Biomolecules have sophisticated functions, such as catalysis, molecular recognition and self-restoration. In order to combine these functions with solid-state devices and realize a novel bio-mimetic device, preferential immobilization of biomolecules onto a chip is required [1–3]. However, the conventional silicon processes, in general, involve harmful conditions for biomolecules, such as high temperature, high vacuum, and extremely low hydrogen potential (pH). Hence, it is essential to develop a new process to immobilize the biomolecules on a chip without losing their activity during the immobilization.

In this paper, we report three bottom-up processes for site-directed covalent immobilization of

* Corresponding author. Tel.: +81 3 5286 3842; fax: +81 3 5272 5749.
E-mail address: tanii@ohdomari.comm.waseda.ac.jp (T. Tanii).

0169-4332/$ – see front matter © 2004 Elsevier B.V. All rights reserved.
doi:10.1016/j.apsusc.2004.05.033

deoxyribonucleic acid (DNA) onto silicon high-density patterns. Electron beam (EB) lithography is performed for the arrangement of amino-terminated areas on a silicon substrate. An organosilane self-assembled monolayer (SAM) is also utilized in order to passivate the outside of the pattern. DNA probes are attached within the amino-modified area with linker molecules. Fluorescent signals from the complementary and non-complementary sequences are obtained in order to compare the hybridization specificity after the immobilization. Although we cannot immobilize various DNA sequences on one chip by this protocol, at least, we confirm that the activity of immobilized DNA is maintained by testing the hybridization specificity. The versatility of the organosilane SAM is also discussed in terms of the fluorescent signal enhancement and the pattern miniaturization.

2. Experimental

We have examined three processes for the site-directed covalent immobilization of DNA onto silicon microstructure patterns. These processes were designed for the arrangement of amino-terminated patterns on a silicon substrate, on which the DNA was immobilized with a linker molecule. Fig. 1 shows

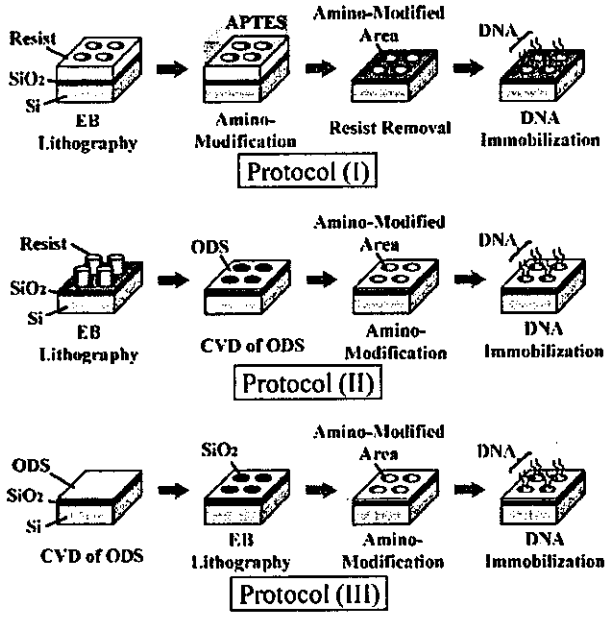

Fig. 1. Schematic representation of DNA immobilization process.

the schematic representation of these processes, respectively. We used silicon substrates covered with thermally grown SiO_2 layer of 10 nm thickness. In the protocol (I), positive resist patterns were prepared by EB lithography. Next, the silicon dioxide surface within the pattern was hydroxylated in a solution of ammonium hydroxide/hydrogen peroxide/water mixture (APM), and terminated with an amino-group by immersing into 2% aminopropyltriethoxysilane (APTES) in 95% acetone/water for 1 h. After the resist removal in organic solvents, the amino-modified substrates were immersed into a solution of 1.25% glutaraldehyde in water for 1 h. Small droplets of complementary and non-complementary oligonucleotides diluted to a final concentration of 20 μM were deposited manually on the surface of the patterns. Then, the substrates were incubated at 38 °C for 2 h in a humidified hybridization chamber, and washed in a buffer. Finally, the DNA-modified surface was exposed to 10 μM of 5′-Cy-5 labeled DNA complement in a buffer, and allowed to hybridize at 65 °C for 2 h. The hybridized surface was rinsed once in a buffer for 5 min to remove any non-hybridized complement.

Complementary and non-complementary oligonucleotides to be immobilized on to microstructure patterns as probe DNA were amino-modified at 5′ end, and oligonucleotides employed for target DNA were Cy-5 labeled at 5′ end. Each of these oligonucleotides was 21 mer in length. The sequences were H_2N-5′-CCACGGACTACTTCAAAACTA-3′ (complementary probe), H_2N-5′-ATCGATCGAT-CGATCGATCGA-3′ (non-complementary probe) and Cy-5-5′-TAGTTTTGAAGTAGTCCGTGG-3′ (target), respectively.

In the protocol (II), we have improved the immobilization process by using organosilane SAM passivation. In this procedure, the negative resist patterns on a silicon dioxide substrate were prepared. After the treatment in APM, the silicon dioxide surface was covered with an octadecyltrimethoxysilane (ODS)-SAM by means of a chemical vapor deposition (CVD) [4]. The CVD was performed at 110 °C for 4 h. It was previously reported that this CVD method produced a high-uniformity SAM [5,6]. Since the ODS-SAM produced a hydrophobic surface, it was expected that this passivation layer prevented the unintended adsorption of molecules during the process. Following the CVD of ODS, we immersed the

substrates into 10 μM ethyltriethoxysilane (ETS) in ethanol for 1 h. The effectiveness of this immersion is discussed later. Finally, the negative resist pattern was completely removed, and the patterns were modified with APTES. Then, the substrates were baked at 150 °C in order to evaporate the adsorbing molecules. The immobilization and the hybridization of DNA were performed in the same way as the protocol (I).

The protocol (III) was designed taking full advantage of ODS-SAM. In this procedure, ODS-SAM served as a resist film for EB lithography as well as the passivation layer. Following the CVD of ODS and subsequent ETS modification, EB lithography was performed directly onto SAM. It has been reported that nano-scale patterns could be achieved by EB lithography onto ODS-SAM, because the pattern expansion due to the proximity effect was negligible [7]. It was also possible to fabricate microstructure patterns on ODS-SAM by means of vacuum ultraviolet (VUV) photolithography, as described in the previous reports [4–6]. We have performed EB lithography using buffered hydrofluoric acid (BHF) as a developer. The EB energy was 20 keV, and the dose was 960 μC/cm^2. By immersing into a solution of HF:NH_4F:H_2O (1:4:180) for 60 s, the irradiated region was developed completely. Then, the exposed silicon dioxide region within the pattern was modified with APTES. It was also reported that ODS was resistant to BHF immersion and served as a mask for the pattern transfer into underlying SiO_2 layer [8–10]. The immobilization and the hybridization processes were carried out as mentioned above. Finally, the array of DNA labeling target DNA bound to the capture DNA immobilized on the microstructure pattern was observed in a fluorescent microscope with a He–Ne laser (1.0 mW, 632.8 nm).

3. Results and discussion

In the protocol (I), we have examined the efficiency of DNA immobilization onto amino-modified area arranged on the silicon dioxide surface. Because the conditions for EB lithography onto conventional resist have been well known, it was the easiest to begin with this process. Fig. 2 shows the fluorescent images of hybridization of the target DNA labeled with Cy-5 to the complementary and non-complementary DNA

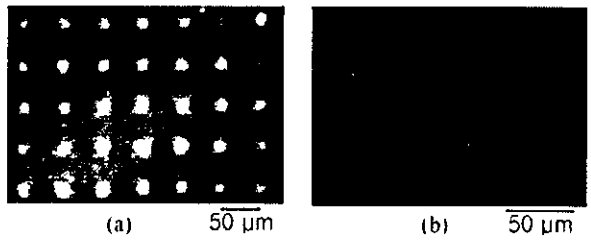

Fig. 2. Fluorescent images of target DNA labeled with Cy-5 hybridized to the probe DNA immobilized within the microstructure patterns by protocol (I) (size: 10 μm, pitch: 50 μm). (a) Complementary DNA immobilized within the microstructure patterns. (b) Non-complementary DNA immobilized within the microstructure patterns.

immobilized within the microstructure patterns. As shown in Fig. 2, it is clear that the fluorescent signals corresponded to the strong binding of fluorophore-labeled DNA to the immobilized DNA within the pattern. This result indicates that the amino-modified oligonucleotides were indeed attached to the microstructure patterns and were accessible to the target DNA. We also confirmed that the fluorescent signal was not due to the unspecific binding of the Cy-5-labeled DNA onto the immobilized probe DNA, because no binding was observed from non-complementary probes as shown in Fig. 2. However, the fluorescent signals exhibited irregular shapes. Almost all the patterns seemed expanded compared to the original rectangular shape with sides 10 μm long. By taking atomic force microscopy (AFM) images of the amino-modified patterns, we have confirmed that this pattern expansion was due to the diffusion of APTES during the resist removal. It is considered that APTES stuffed in the resist openings diffused and bound onto the SiO_2 surface around the pattern. As a result, we could not detect any fluorescent signal from denser patterns. That was why we intended to cover the outside of the pattern with an inert passivation layer.

In the protocol (II), the outside of the amino-modified area was covered with organosilane beforehand. In addition to the ODS-SAM deposition, we exposed the substrates to ETS for the passivation. ETS is a relatively small silane compared to ODS. Table 1 shows the effectiveness of the ETS treatment. In this test, bare SiO_2 surface without any patterns was modified in APM, ODS, ETS and APTES in turn. The check marks in Table 1 indicate that the wafer has been exposed to that reagent. The ODS-SAM surface

Table 1
Water contact angle of the wafer at each process step

Process step wafer no.	1. APM	2. ODS	3. ETS	4. APTES	Water contact angle
No. 1	✓				~0 ° (Hydrophilic)
No. 2	✓	✓			111 ° (Hydrophobic)
No. 3	✓	✓	✓		91 ° (Hydrophobic)
No. 4	✓	✓		✓	44 ° (Hydrophilic)
No. 5	✓	✓	✓	✓	81 ° (Hydrophobic)

exhibited hydrophobic surface with the contact angle of 111 °C. Comparing the water contact angle of wafer number 2 with that of number 4, it is clear that the surface returned to hydrophilic again after the subsequent APTES modification. This degradation was thought to be due to adsorption of APTES onto ODS-SAM, because APTES was relatively small compared to ODS. This adsorption resulted in poor selectivity in immobilization of DNA between inside and outside the pattern. We could solve this problem by immersing the ODS-SAM into ETS. As shown in Table 1, the ODS-SAM exposed in ETS kept its hydrophobic surface after APTES treatment (wafer number 5). Because ETS is the smallest, the available sites for APTES to adsorb in ODS-SAM have already been filled with ETS, and the surface stayed hydrophobic during APTES treatment. As a result, we could immobilize DNA only inside the pattern. Fig. 3 shows the fluorescent images of target DNA, bound to the complementary probe on the microstructure patterns. The fluorescent images exhibited the regular shape. In addition, we could detect the fluorescent signals also from nanostructure patterns as shown in Fig. 3b. Fig. 4 shows the fluorescent image of 1 μm pattern at intervals of 10 μm. As shown in Fig. 4, however, many speckled background noises were recognized on the substrates prepared by protocol (II). The area is delineated with broken lines also in Fig. 3. This indicates that the remainder of the conventional EB resist was hardly removed in an organic solvent, if it was applied to organosilane SAM and caused the background noise in the fluorescent images.

While the protocol (II) was elaborated and relatively complicated, the protocol (III) was a simple and self-aligned process that enabled us to perform the amino-modification and the passivation simultaneously. Fig. 5 shows the fluorescent image of the Cy-5 labeled DNA hybridized to the complementary probe immobilized on the substrate by means of protocol (III). The fluorescent image shown in Fig. 5 exhibited good uniformity with no speckled background noise. It has also been confirmed by a performance test of our handmade fluorescent microscope that the relatively bright region in the outside of the pattern in Fig. 5 is mainly due to the non-uniformity of the laser intensity. Thus, it is clear that the speckled background noise was due to the conventional EB resist. We need further spectroscopic analysis in order to clarify whether the remainder of the DNA was still adsorbed on the SAM surface in the outside of the

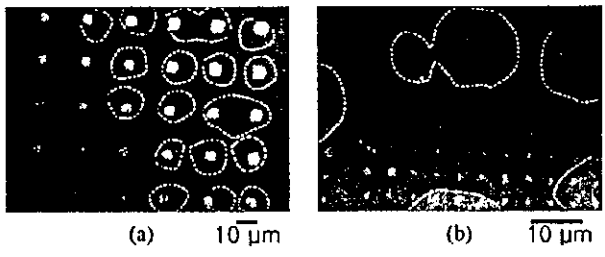

Fig. 3. Fluorescent images of target DNA labeled with Cy-5 hybridized to the complementary probe DNA immobilized by protocol (II). (a) Microstructure patterns (size: 5 μm, pitch: 20 μm). (b) Nanostructure patterns (size: 500 nm, pitch: 5 μm).

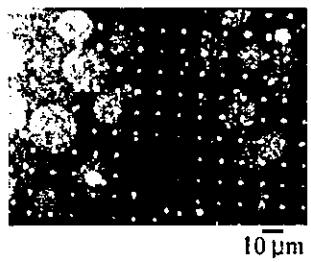

Fig. 4. Speckled background noises in the fluorescent image of Cy-5-labeled DNA hybridized to probe DNA immobilized by protocol (II) (size: 1 μm, pitch: 10 μm).

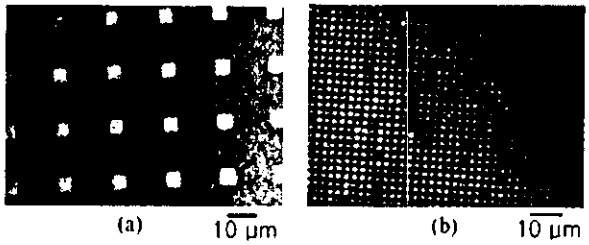

Fig. 5. Fluorescent image of Cy-5-labeled DNA hybridized to the complementary probe DNA immobilized on the ODS-SAM patterns by protocol (III). (a) Microstructure patterns (size: 5 μm, pitch 20 μm). (b) Nanostructure patterns (size: 250 nm, pitch 2.5 μm). The relatively bright region in the outside of the pattern is mainly due to the non-uniformity of laser intensity in our handmade fluorescent microscope.

pattern or not. However, it is concluded that the adsorption was negligible because we could obtain a high-density fluorescence pattern according to the high uniformity and the high contrast as shown in Fig. 5b. Therefore, the protocol (III) has the advantage of high fluorescent signal to noise ratio.

4. Conclusion

We have proposed new processes for site-directed immobilization of DNA onto microstructure patterns and demonstrated the fluorescent observation of fluorophore-labeled DNA hybridized to complementary and non-complementary probe DNA immobilized onto the patterns. Three protocols were examined by comparing the fluorescent signals. By taking advantage of the versatility of ODS-SAM, we have succeeded in obtaining regular and uniform fluorescent signals from the DNA immobilized on micro and nanostructure patterns. It has been confirmed that the proposed protocols are effective for site-directed immobilization of amino-modified biomolecules onto silicon fine structures. This technique is also powerful for the biochip development and the chip miniaturization.

Acknowledgements

This work is supported by a Grant-in-Aid for Center of Excellence (COE) Research from Ministry of Education, Culture, Sports, Science and Technology, and by a Grant for the Graduate Schools from the Promotion and Mutual Aid Corporation from Private Schools of Japan.

References

[1] J. Reichert, A. Csaki, R. Moller, J.M. Kohler, W. Fritzsche, Anal. Chem. 72 (2000) 6025.
[2] M. Veiseh, M.H. Zareie, M.Q. Zhang, Langmuir 18 (2002) 6671.
[3] S.P.A. Fodor, Science 277 (1997) 393.
[4] H. Sugimura, K. Ushiyama, A. Hozumi, O. Takai, Langmuir 16 (2000) 885.
[5] K. Hayashi, N. Saito, H. Sugimura, O. Takai, N. Nakagiri, Langmuir 18 (2002) 7469.
[6] A. Hozumi, Y. Yokogawa, T. Kameyama, H. Sugimura, K. Hayashi, H. Shirayama, O. Takai, J. Vac. Sci. Technol., A 19 (2001) 1812.
[7] C.S. Whelan, M.J. Lercel, H.G. Craighead, K. Seshadri, D.L. Allara, Appl. Phys. Lett. 69 (1996) 4245.
[8] T. Komeda, K. Namba, Y. Nishioka, J. Vac. Sci. Technol., A 16 (1998) 1680.
[9] T. Komeda, K. Namba, Y. Nishioka, Jpn. J. Appl. Phys. 37 (1998) L214.
[10] T. Komeda, K. Namba, Y. Nishioka, Appl. Phys. Lett. 70 (1997) 3398.

Japanese Journal of Applied Physics
Vol. 44, No. 9, 2005, pp. L295–L298

Micropatterning Oligonucleotides on Single-Crystal Diamond Surface by Photolithography

Guo-Jun ZHANG[1,*], Hitoshi UMEZAWA[2,†], Hideo HATA[2], Tamotsu ZAKO[3], Takashi FUNATSU[3], Iwao OHDOMARI[1,2,4] and Hiroshi KAWARADA[1,2]

[1]*Nanotechnology Research Center, Waseda University, 513 Waseda Tsurumaki-cho, Shinjuku-ku, Tokyo 162-0041, Japan*
[2]*Department of Electronical Engineering and Bioscience, School of Science and Engineering, Waseda University, 3-4-1 Okubo, Shinjuku-ku, Tokyo 169-8555, Japan*
[3]*Laboratory of Bio-Analytical Chemistry, Graduate School of Pharmaceutical Sciences, The University of Tokyo, 7-3-1 Hongo, Bunkyo-ku, Tokyo 113-0033, Japan*
[4]*Kagami Memorial Laboratory for Materials Science and Technology, Waseda University, 2-8-26 Nishi-waseda, Shinjuku-ku, Tokyo 169-0051, Japan*

(Received November 1, 2004; accepted December 31, 2004; published February 10, 2005)

DNA micropatterns have been for the first time fabricated on a single-crystal diamond surface in conjunction with the photolithography technique. A new chemical modification process for producing amine groups inside patterned regions and a passivation layer terminated with fluorine outside patterned regions is demonstrated. The resulting amine groups within patterned areas and fluorine termination outside patterned areas on the single-crystal diamond surface were characterized by spatially resolved X-ray photoelectron spectroscopy. Amine-terminated oligonucleotides were then linked to the amine-patterned regions using a crosslinker. It was revealed that hybridization on DNA-patterned diamond is specific and selective, with a low background outside the patterns and strong binding to complementary probe DNA immobilized inside the patterns but no binding to noncomplementary probe DNA similarly immobilized inside the patterns. These results suggest that DNA micropatterning on a single-crystal diamond may serve as an ideal platform for future biochips and biosensors.
[DOI: 10.1143/JJAP.44.L295]

KEYWORDS: DNA, immobilization, microstructures, hybridization, single-crystal diamond, photolithography

Much attention has been given to the combined use of microelectronics and biotechnology to develop integrated biosensing systems such as DNA on Au electrodes,[1] DNA on fiber optics[2] and proteins on fiber optics.[3] Among the microelectronics-compatible materials such as glass, silicon, gold and diamond, diamond is a remarkable material due to its high chemical stability,[4,5] high sensitivity in electrochemical reaction,[6] and biocompatibility.[7,8] Therefore, diamond is an ideal substrate for the integration of microelectronics with biological molecules. DNA attachment on diamond surfaces involving polycrystalline diamond and nanocrystalline diamond has already been established.[9–12] However, only a few methods of chemically modifying diamond surfaces for biomolecular immobilization have been investigated due to the absence of well-defined chemical groups on diamond surfaces.[9–14] More recently, DNA-modified nanocrystalline diamond thin films have been demonstrated as stable and biologically active substrates for the integration of microelectronics with biological modification and sensing.[9] However, it is still difficult to precisely make clear chemical modification process on such a thin film while chemical functionalization is conducted on nanocrystalline diamond. Single-crystal diamond is flat and highly pure, enabling us to fully understand the chemical changes on the surface. Here, we present a new approach in micropatterning DNA on a chemically modified single-crystal diamond surface by photolithography. Our results show that the shapes of the micropatterns are well controlled using this surface-patterning technique, and DNA deposition on micropatterns is precise and uniform; likewise, the subsequent hybridization process shows high selectivity and specificity.

*E-mail address: zhang@kaw.comm.waseda.ac.jp
†E-mail address: umezawa@kaw.comm.waseda.ac.jp

The strategy for the fabrication of micropatterns on a single-crystal diamond surface is outlined in Fig. 1, which involves many steps: single-crystal diamond has a relatively flat surface with a mean roughness of less than 10 nm. Single-crystal diamond Ib (001) was heated to 800°C with 750 W coupled hydrogen plasma for 30 min to terminate the surface with hydrogen (Fig. 1(b)). The hydrogen-terminated surface has a p-type conductive layer and shows unique properties, leading to a number of potential applications.[15] The oxidization of the diamond surface was performed by exposing the hydrogen-terminated diamond samples to ultraviolet light and ozone for 1 h.[4] After treatment with ozone, the hydrogen-terminated surface most likely changes to a surface containing ether and hydroxyl groups, resulting in the surface-functionalized groups (Fig. 1(c)). An approximately 100-nm-thick Au film was deposited on the oxidized diamond surface as a mask and another resist film was then coated on the gold layer (Fig. 1(d)). The negative patterns were fabricated by photolithography, which obtained by etching off the gold using a solution containing KI and I_2 (Fig. 1(e)). After removing the resist film, the etched areas were exposed to C_3F_8 plasma using inductively-coupled plasma (ICP) for 20–30 s to generate a fluorine-terminated surface, which is a hydrophobic surface capable of minimizing the subsequent unspecific binding of biomolecules (Fig. 1(f)). The micropatterns with feature sizes as small as 5 μm were finally realized by etching off the remnant gold mask on the surface.

The resulting micropatterns indicate that there is a hydrophilic surface inside the feature where the functionalized groups still remain, and another hydrophobic surface in the region between the features that is terminated with fluorine, enabling easy filling of the micropatterns with an aqueous solution containing biomolecules of interest. To provide chemically reactive amine groups, the hydrophilic